

Cenozoic exhumation history of the Alborz Mountains, Iran: New constraints from low-temperature chronometry

M. Rezaeian,¹ A. Carter,² N. Hovius,³ and M. B. Allen⁴

Received 25 June 2011; revised 18 January 2012; accepted 19 January 2012; published 16 March 2012.

[1] The Alborz Mountains in the north of the Turkish-Iranian Plateau mainly developed in the Cenozoic as a consequence of the closure of Neo-Tethys and continental collision between Arabia and Eurasia. Cenozoic growth of the fold-and-thrust belt exploited an older Palaeozoic-Mesozoic crustal fabric but the extent to which this governed the overall form of the mountain belt is unclear. To determine when and how the Alborz mountain belt has grown, apatite fission track (AFT) and (U-Th)/He (AHe) thermochronometry were performed on 46 bedrock samples collected along 8 transects across the range. AFT central ages range from 157 ± 24 Ma to 10 ± 1 Ma with most ages falling between 40 Ma and 10 Ma. AHe ages range from 17 ± 2 Ma to 6 ± 1 Ma. The data revealed enhanced exhumation ca. 35 ± 5 Ma, minor exhumation between ca. 30–20 Ma and an increase in exhumation thereafter. This pattern matches the tripartite Mid-Cenozoic stratigraphy of Central Iran, where Upper Oligocene-Lower Miocene carbonates are sandwiched between terrestrial clastic formations. The most intriguing thermochronometric signal found is a major acceleration of exhumation that initiated in the late Miocene to early Pliocene, recorded by the AHe data. There does not appear to be a direct tectonic cause for Pliocene intensified erosion, as convergence rates between Arabia and Eurasia have remained relatively constant. Enhanced exhumation at this time may reflect a climatically induced intensification of erosion during Caspian isolation and base level fall, or a regional tectonic re-organization of the Arabia-Eurasia collision, or both.

Citation: Rezaeian, M., A. Carter, N. Hovius, and M. B. Allen (2012), Cenozoic exhumation history of the Alborz Mountains, Iran: New constraints from low-temperature chronometry, *Tectonics*, 31, TC2004, doi:10.1029/2011TC002974.

1. Introduction

[2] The narrow (≤ 120 km), high (max elevation 5628m) Alborz mountain belt located in northern Iran adjacent to the South Caspian Basin (SCB) (Figure 1) is a doubly vergent orogen formed along the northern edge of the Turkish-Iranian Plateau in response to the closure of the Neo-Tethys Ocean and continental collision between Arabia and Eurasia. Ocean closure began in the Late Cretaceous-Early Tertiary [Berberian and King, 1981; Berberian, 1983; Şengör, 1990; Ziegler, 2001] since when there has been ca. 1400–1600 km of convergence between Arabia–Eurasia [McQuarrie *et al.*, 2003]. At the longitude of the Alborz range, current deformation related to the collision is accommodated almost equally in three main regions: the Zagros, the Alborz and the Apsheron-Balkan sill (ABS), and shortening across the

Alborz accounts for ca. 30% of the current 22 mm yr^{-1} convergence between Arabia and Eurasia (Figure 1) [Vernant *et al.*, 2004]. However, there is variation in strain along the range, and strike-slip deformation dominates in the east whereas thrusting is more commonplace to the west [Djamour *et al.*, 2010].

[3] The Alborz Mountains show significant along strike changes in mountain belt width, topographic slope, symmetry and structures that presumably reflect trends in climate and/or tectonics. At the regional scale the mountains are affected by sharp orographic asymmetry with a wet north side (precipitation up to 1800 mm yr^{-1} (Tahghighat Manabe AB, unpublished data, monitored up to year 2000 with an average period of record of 25 years), capturing water vapor sourced from the adjacent Caspian Basin, and a semi-arid south side. The north flank of the Alborz (where flank means a side of the main drainage divide) has steep topographic slopes and significant relief, rising above the coastal plains at the edge of the Caspian Sea (-29 m a.s.l.), compared to the gentler slopes and lower relief of the southern flank which is connected to the elevated Central Iranian Plateau (1500 m a.s.l.).

[4] A systematic variation in topographic taper of the mountain belt from east to west coincides with structural trends. East of $\sim 52^\circ 30' \text{E}$ (Figures 2, areas a and b) the north

¹Department of Earth Sciences, Institute for Advanced Studies in Basic Sciences, Gava Zang, Zanjan, Iran.

²Department of Earth and Planetary Sciences, Birbeck, University of London, London, UK.

³Department of Earth Sciences, University of Cambridge, Cambridge, UK.

⁴Department of Earth Sciences, Durham University, Durham, UK.

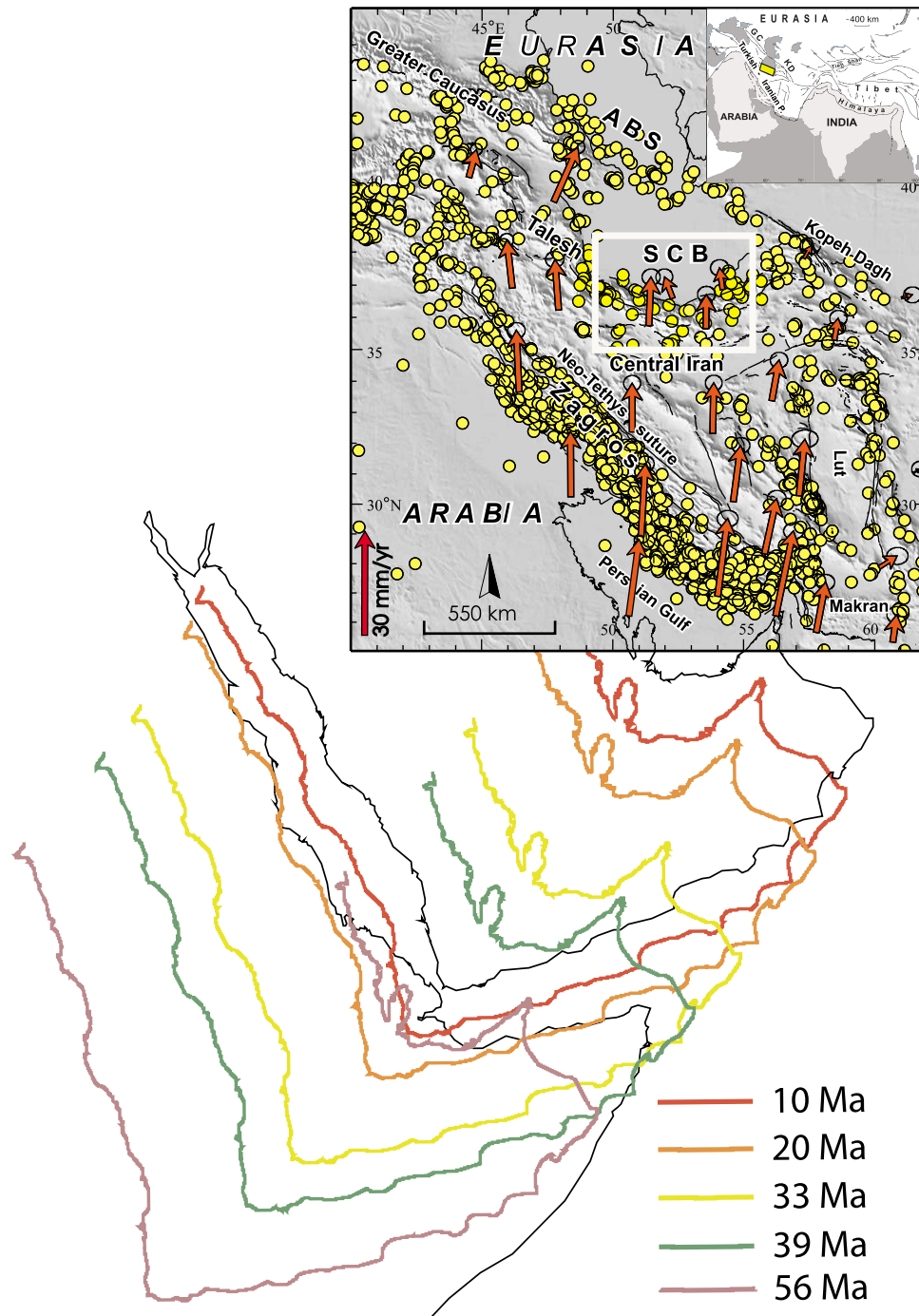


Figure 1. Reconstruction of plate convergence for Arabia-Eurasia collision since the Early Cenozoic [McQuarrie *et al.*, 2003; Hatzfeld and Molnar, 2010] with the location of the Alborz Mountains, marked by a white box. The inset shows the present location within Turkish-Iranian Plateau of Alpine-Himalayan belt shown in the box. The present location of the Zagros Mountains, the Neo-Tethys suture, Central Iran, Talesh, Kopet Dagh, Greater Caucasus, South Caspian Basin (SCB), Apsheron-Balkhan Sill (ABS) and the Alborz within the collision zone are defined. The boundaries between the Turkish-Iranian Plateau and stable adjacent Arabia-Eurasia platforms have been shown by the location of teleseismically recorded earthquakes in a period of 1964–2004 from Tatar *et al.* [2007]. The position of the Arabian plate between 56 and 10 Ma has been displayed by colored lines and the present, GPS-derived velocity field of the collision zone, with respect to stable Eurasia by the red arrows [Vernant *et al.*, 2004].

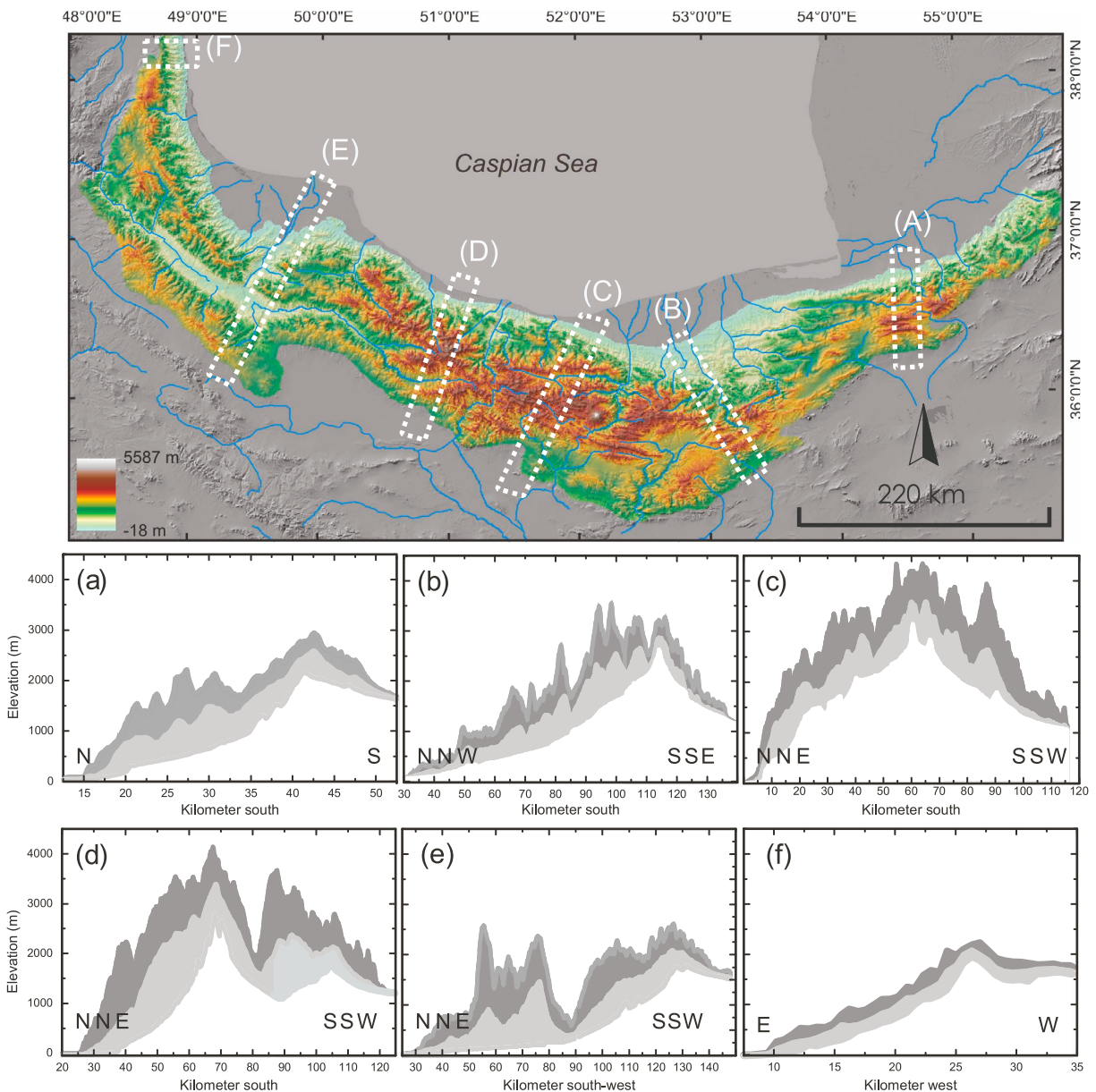


Figure 2. Topographic cross sections of the Alborz Mountains illustrating the typical two-sided geometry of the mountain belt. Areas a and b are in the eastern Alborz with NE-SW structural trend; area c is in the central Alborz with E-W structural trend; areas d and e are in the west-central Alborz with NW-SE and E-W structural trends; and area f is in the western Alborz with N-S structural trends. Plotted at 500 m intervals are the maximum, mean, and minimum elevations along 20-km-wide swath profiles taken from the SRTM DEM. Horizontal axis is the distance from Caspian Sea coastline in kilometers. The geometry of the Alborz changes from an asymmetric double-sided wedge in the east (areas a and b) to a more or less symmetric double-sided wedge in the center (area c), and an asymmetric double-sided wedge with a second, smaller range to the south, in the center-west, and single asymmetric double-sided wedge in the west (areas d, e, and f).

flank of the mountain belt is > 4.5 times wider than the south flank, and deformation is characterized by left-lateral strike-slip faulting while thrusting occurs at lower rates [Djamour *et al.*, 2010]. West of $52^{\circ}30'$ E (Figure 2, areas c, d, and e), the structural trend changes from ENE-WSW to the WNW-ESE. In the north flank of the mountain belt, between $50^{\circ}00'$ and $52^{\circ}30'$ E, the structures include foreland-dipping (N) thrusts [Allen *et al.*, 2003]. Finally, west of $49^{\circ}00'$

(Figure 2, area f) there is a return to strong topographic asymmetry, but here the southeast flank is up to seven times wider than the northwest flank of the mountain belt. Along the range, the north side of the Alborz has a relatively simple range front that borders the South Caspian Basin. The southern side is less regular, with isolated fault blocks situated south of the main range (Figure 3).

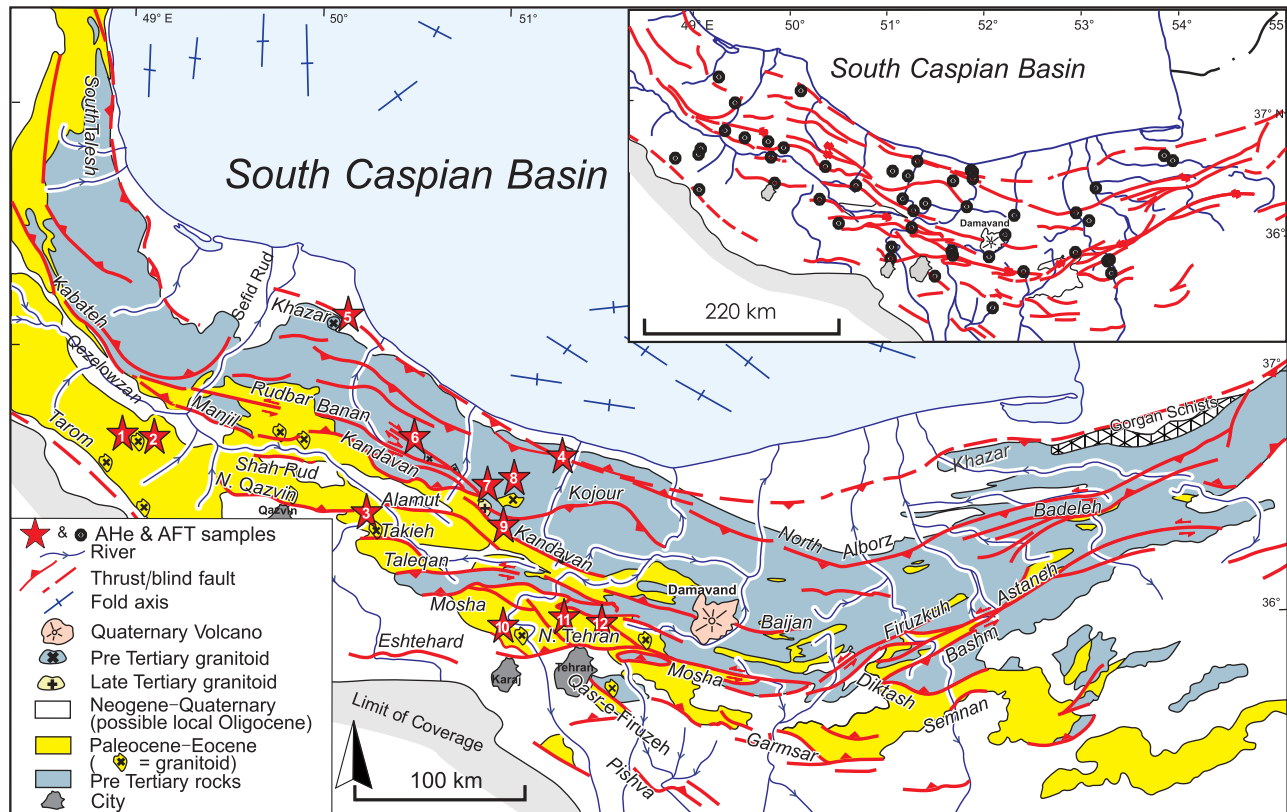


Figure 3. Geological map showing the main rock units and structures within the Alborz Mountains and adjacent area after *Allen et al.* [2003] (with permission from Elsevier) [*Berberian et al.*, 1985, 1996; *Berberian and Yeats*, 2001; *Jackson et al.*, 2002; *Guest et al.*, 2006b]. Red stars give the location of apatite (U-Th)/He samples used in this study. Inset: A simplified structural map of the Alborz including AFT sample location in black circles and main faults (red lines) to show the structural location of the sampled rocks.

[5] While the form of the mountain belt relates to contrast between a rigid South Caspian basement and deformation of a zone of weak crust (Alborz) through reactivation of inherited Paleozoic-Mesozoic crustal fabrics [e.g., *Guest et al.*, 2006a; *Zanchi et al.*, 2006; *Yassaghi and Madanipour*, 2008] the extent to which tectonics, inherited structure and climate have exerted control on orogenic development has not yet been quantified. Current geodetic shortening rates of the Alborz are 15% and 30% of the rates recorded in the Andes and the Himalaya, respectively [*Bilham et al.*, 1997; *Liu et al.*, 2000], but translation of the shortening rates to strain rates, taking into account the width of the deformation zones, shows that the strength tectonic forcing in the Alborz is comparable to these larger mountain belts.

[6] During the early Cenozoic, the geology of the area that now forms the southern flank of the Alborz was closely linked to the deformation that affected Central Iran [*Stöcklin*, 1968], while the northern region was more influenced by events in remnant Para-Tethys. It has been proposed that both areas only started behaving as a coherent tectonic unit since the early Pliocene associated with a widespread tectonic re-organization in the Arabia-Eurasia collision zone [e.g., *Axen et al.*, 2001a; *Allen et al.*, 2004]. To understand this progression in more detail, and to elucidate the Cenozoic exhumation history of the Alborz Mountains, we have

conducted a low temperature chronometry study of bedrock samples collected across the entire mountain belt, encompassing areas that show changes in taper and topographic symmetry.

2. Regional Geology

[7] The Alborz Mountains, situated 200–500 km to the north of the Neo-Tethyan suture in the Arabia-Eurasia collision zone, are a product of convergence between the domains of Central Iran and the South Caspian Basin-Eurasia. Deformation within the Alborz is governed by main frontal thrust faults at its borders and strike-slip faults at relatively high elevation within the range [*Tatar et al.*, 2007]. The Khazar Fault (Figure 3) is interpreted to define the structural boundary between the Alborz and the South Caspian basin. If so, then the fault plane imaged from the aftershock pattern following the 2004 Baladeh earthquake (Mw = 6.2; 10–30 km depth) [*Tatar et al.*, 2007] indicates southwards underthrusting of the South Caspian basement. Recent modeling of current interseismic deformation in the Alborz suggests that there are major differences in strain partitioning and by implication deformation pattern across the range [*Djamour et al.*, 2010]. While a large part of the Alborz mountain belt is located above the seismically coupled part of the Khazar Fault (dip 34 degrees

to the south with a locking depth of ~ 30 km), the main bounding faults in the southern part of the Alborz have a different geometry (85 degree dip to the north, locking depths up to 16 km) [Djamour *et al.*, 2010]. Whether this pattern of strain partitioning has persisted over the geological long-term is unknown.

[8] Most of the well-constrained earthquakes in the Alborz have occurred at depths < 15 km, with either reverse focal mechanisms or left lateral strike-slip on longitudinal faults [Jackson *et al.*, 2002]. A minor normal deformation component has been recognized in seismic data and geological observations mainly in the south central Alborz [Ashtari *et al.*, 2005; Guest *et al.*, 2006a; Ritz *et al.*, 2006; Landgraf *et al.*, 2009]. Whether this extension is local or regional in significance is not yet clear due to lack of high resolution geodetic data but existing GPS measurements indicate differential rates of shortening along the range as a whole. Maximum rates of slip are recorded by GPS stations on the Khazar Fault (~ 6 mm/yr of shortening and ~ 5 mm/yr of left lateral strike slip to the west and east, respectively.), implying that most of the shortening occurs in the NW of the range [Djamour *et al.*, 2010], or by underthrusting of the South Caspian Basin beneath the Alborz.

[9] A generalized geological map of the Alborz Mountains, with the location of principal structures and geographic names is shown in Figure 3, and the Cenozoic stratigraphy of the Alborz region is outlined in Figure 4. The stratigraphy contains a series of unconformities that mark episodes of discrete rock uplift and erosion and/or non-deposition, which are overlain by terrestrial clastic rocks recording abrupt changes in sediment accumulation rate, grain size, and clast composition. The key events reflected by the regional geology are summarized below (Figure 4).

[10] Paleocene (~ 60 Ma): An early Alborz was emergent in the Early Tertiary [e.g., Stöcklin, 1968; Clark *et al.*, 1975; Sussli, 1976; Berberian, 1983], and some surface uplift may have taken place as early as the Middle Mesozoic in the northern Alborz region [Sussli, 1976; Salehi Rad, 1979]. An erosional unconformity is present at the base of the Cenozoic sequence in the south flank of the present mountain belt. It reflects the onset of substantial compressional deformation throughout much of the Turkish-Iranian Plateau [e.g., Berberian, 1983; Guest *et al.*, 2006a]. This compression phase predates the initial Arabia-Eurasia collision and is likely to be related to the closure of small oceanic basins within the collision zone of southern Iran.

[11] Eocene (~ 55 – 34 Ma): Subduction related magmatism (voluminous intermediate silicic to calc-alkaline and shoshonitic types) in the back arc of the Neo-Tethys subduction zone [Berberian and King, 1981]. Associated crustal extension caused subsidence of the region, which now forms the southern Alborz, whereas the northern part of the present mountain belt was a geographic high [Berberian and King, 1981]. The extension was paired with widespread submarine volcanism, represented in the regional stratigraphy by a thick (3–9km) sequence of volcanics and volcanoclastic sediments [Verdel *et al.*, 2011] (Figure 4). These materials were deposited in a rapidly subsiding back-arc basin linked to rollback of the Neo-Tethys slab [Vincent *et al.*, 2005; Verdel *et al.*, 2011]. Volcanism was at its most intense in the Middle Eocene (~ 40 Ma) [e.g., Emami, 2000].

[12] Late Eocene-Early Oligocene (~ 34 Ma): Submarine volcanoclastic sedimentation ended as the tectonic regime reverted to compression. The timing of this change is consistent with a regional termination of the voluminous arc and back-arc magmatism [Ballato *et al.*, 2011] across Iran and adjacent areas, related to the initial collision of Arabia and Eurasia [Allen and Armstrong, 2008]. At this time the southern Alborz emerged above sea level and was affected by widespread erosion, terrestrial deposition and limited subaerial basaltic volcanism [Stöcklin and Eftekhari-Nezhad, 1969; Anells *et al.*, 1975; Clark *et al.*, 1975; Emami, 2000; Verdel *et al.*, 2011]. This transition from extension to compression affected most of the Arabia-Eurasia collision zone and is recorded by a regional unconformity seen in the Central Iranian Plateau, Turkey, Caucasus, Talesh and Zagros mountains [Hessami *et al.*, 2001; Brunet *et al.*, 2003; Vincent *et al.*, 2007; Morley *et al.*, 2009].

[13] Early Miocene (~ 23 – 16 Ma): Through the Early Miocene (and since the Late Oligocene for some areas) most of central and northern Iran was covered by a shallow epicontinental sea (Qom Sea) and up to 1km of carbonates were deposited [Daneshian and Ramezani Dana, 2007; Reuter *et al.*, 2009]. Their remnants can be found within the south Alborz near the main drainage divide at elevations > 3000 m a.s.l. [Geological Survey of Iran, 2001]. Sediment accumulation rates in the western Alborz were low during this interval, < 0.05 mm/yr [Guest *et al.*, 2007] (Figure 4), implying tectonic quiescence.

[14] Mid-Miocene (~ 16 Ma): Marine deposition ceased with renewed and enhanced sub aerial erosion in the southern Alborz. Sediment accumulation data show at least a tenfold increase in erosion rates compared to the Early Miocene when Qom carbonates were deposited [Ballato *et al.*, 2008]. Thick (up to 6 km) continental red beds (Upper Red Formation) were deposited in a foreland basin along the southern edge of the rising mountain belt, and marine sediments formed along the northern fringe. Scattered volcanism occurred in the interior of the mountain belt.

[15] Early Pliocene (post 5 Ma): Between 5.6 and 5.5 Ma all regions in the Eastern Para-Tethys including the South Caspian Basin show evidence for a marked sea level fall of at least 50 m [Krijgsman *et al.*, 2010]. From 5.5 Ma onward a major change in the oxygen isotope record of the Atlantic margin of Morocco indicates a dramatic change in Eurasian climate, resulting in much warmer and humid conditions. This changed the hydrological balance and resulted in a widespread transgression in the Mediterranean and the Para-Tethys [Krijgsman *et al.*, 2010]. In the Alborz, the Late Miocene sediments were mostly cut by an erosional unconformity, on top of which Pliocene sediments were deposited. These Pliocene rocks consist of alluvial fan deposits across both the north and south sides of the Alborz, consistent with substantial emergence of a mountain belt. However, the precise timing of onset of alluvial sedimentation is not well known due to a lack of geochronology data. Nor is it clear whether this change was related to a regional tectonic event, regional climate change, a combination of the two, or was simply a diachronous threshold effect as the sourcing of sedimentation changed from distal to more proximal locations during progressive deformation. The thermochronometry data obtained by this study may shed new light on these aspects, especially the nature of the

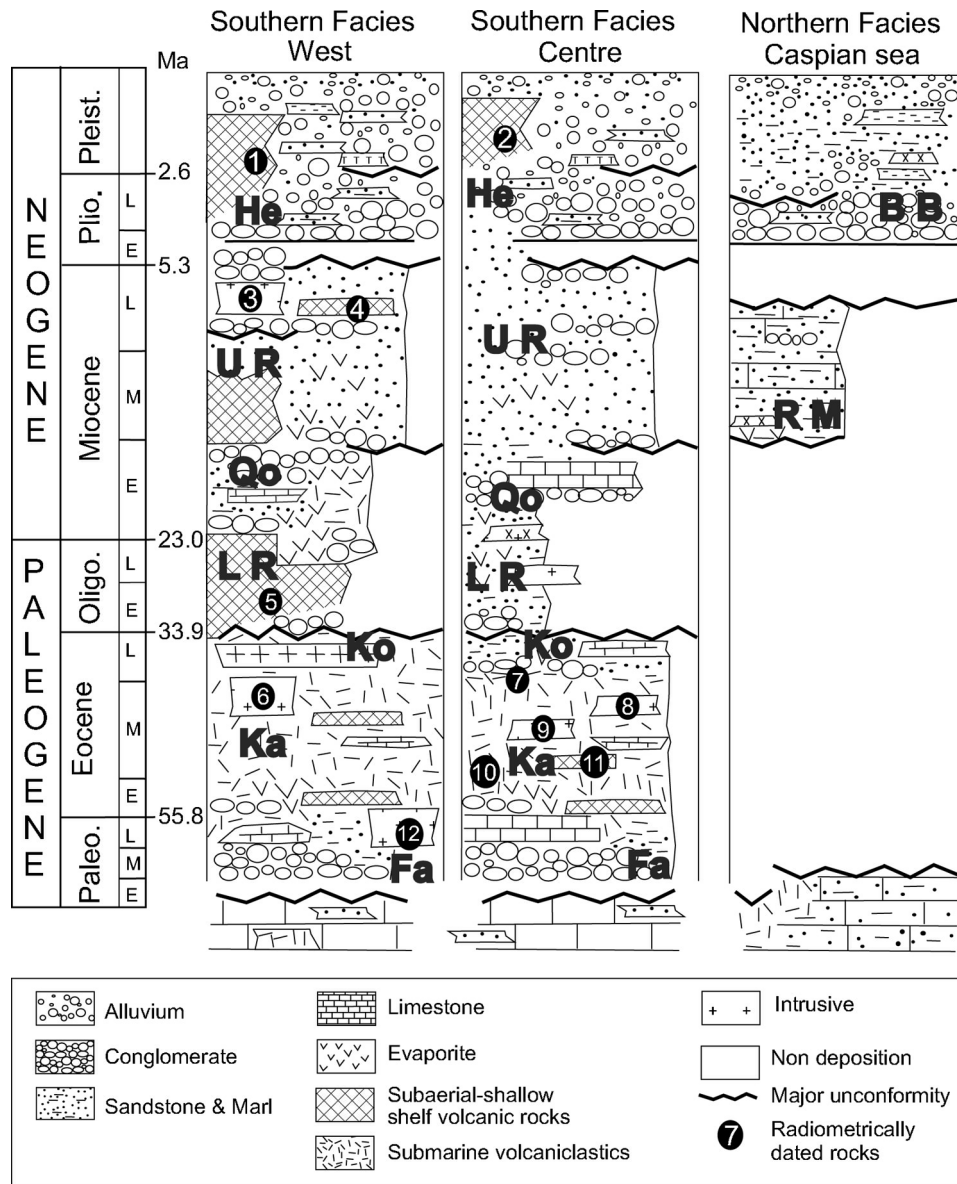


Figure 4. Synthesis of regional stratigraphy after Rezaeian [2008]. Dated units are from N.1 [Guest et al., 2007], N.2 [Davidson et al., 2004], N.3 [Axen et al., 2001a], N.4 and N.5 [Guest et al., 2006b], N.6 [Rezaeian, 2008], N.7 and N.8 [Ballato et al., 2011], N.9 [Davari, 1987], N.10 [Verdel et al., 2011] N.11 [Ballato et al., 2011], and N.12 [Axen et al., 2001a]. The formations of Fajan, Karaj, Kond, Lower Red, Qom, Upper Red, Red Marl, Hezardareh and Brown Bed are labeled as Fa, Ka, Ko, LR, Qo, UR, RM, He and BB, respectively.

transition from an extensional regime in the Eocene to compression in the Oligocene followed by relative tectonic quiescence in the Late Oligocene to Early Miocene. Pinpointing when these changes took place will help understand the underlying causes for these fundamental changes.

3. Methods and Results

[16] To better understand the regional geological record and derive erosion-driven exhumation histories that could reflect changes in the topographic relief of the developing Alborz mountain belt, bedrock samples for thermochronometry analyses were collected from 8 transects

(Figure 5) across the range located along the major transverse valleys draining the north flank of the Alborz to the South Caspian Basin and south flank to Central Iran. Where possible, samples were collected from the valley floors, at ≥ 5 km intervals along each transect, and at smaller intervals near known major thrust faults. Sampled lithologies ranged from fine-grained sandstones to granitoid rocks with stratigraphic or formation ages from Precambrian (2 samples), Paleozoic (5 samples), Mesozoic (20 samples), Paleogene (14 samples) to Neogene (5 samples). The majority of samples are from formations predating presumed Cenozoic shortening and mountain building.

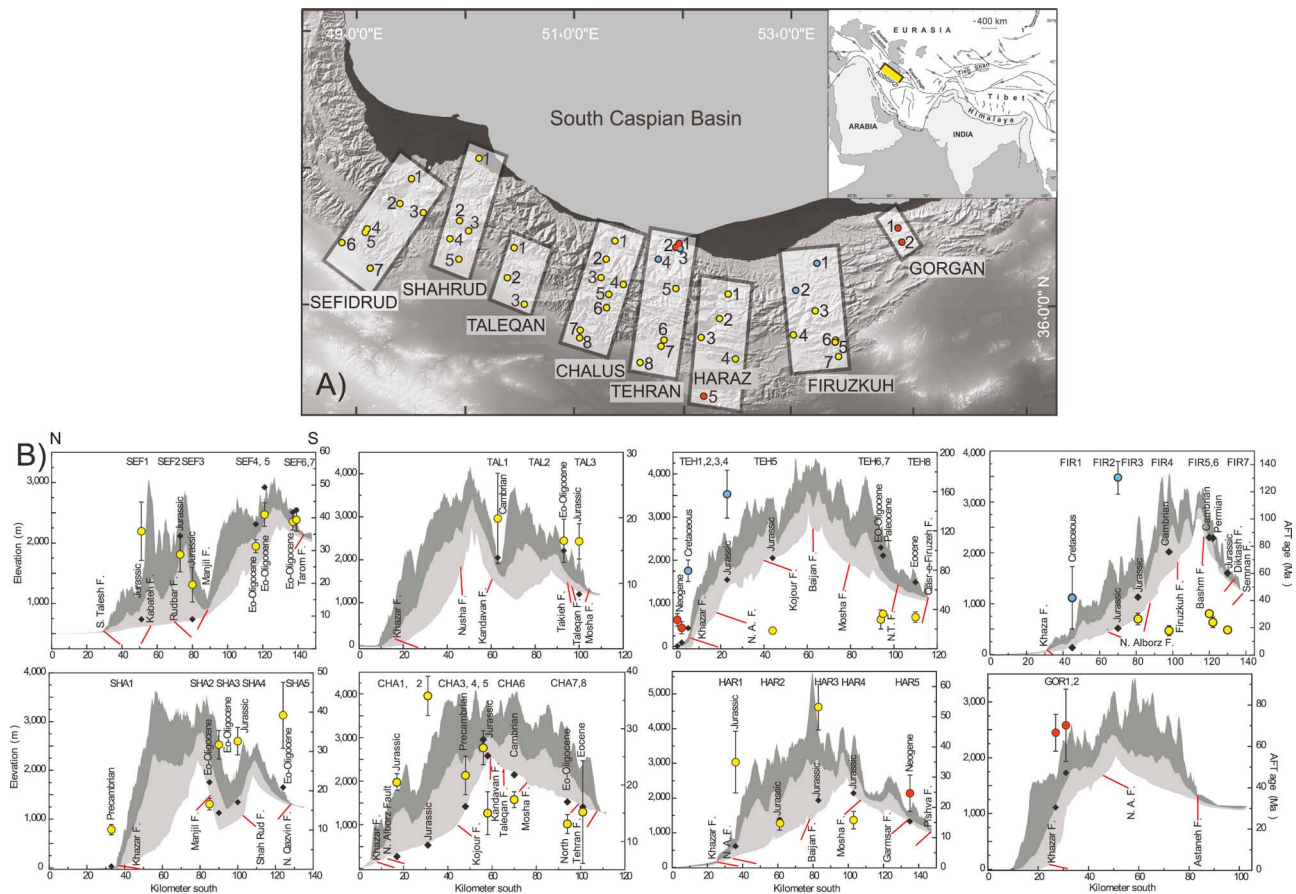


Figure 5. (a) Location of the eight sample transects showing approximate positions of the sampled rocks (colored dots). Partially and un-reset samples are shown by blue and red circles, respectively, fully reset samples are shown in yellow. (b) Topographic cross-sections for each of the sample transects. Maximum, mean and minimum elevations are plotted at 500 m intervals for 20-km-wide swath profiles taken from the SRTM DEM. These transects are named (from E to W) Gorgan, Firuzkuh, Haraz, Tehran, Chalus, Taleqan, Shah Rud and Sefid Rud, and the first three letters were used to prefix sample numbers. Horizontal axis is the distance from Caspian Sea coastline in kilometers. Overlain are locations of the major faults (in red line), AFT ages (yellow, blue and red circles for fully, partially and un-reset samples), stratigraphic ages and sample locations (black diamonds).

[17] Rock samples were analyzed using apatite fission track (AFT) analysis and apatite (U-Th)/He dating (AHe) to determine their low temperature histories (over time-scales >1 Myr) that relate to rock exhumation through the top 2–5 km of the Earth’s crust. Following mineral separation, samples were prepared for fission track analysis and irradiated at the HIFAR nuclear reactor facility in Australia using dosimeter glasses CN-5 to monitor the neutron fluence [Hurford and Green, 1983]. After irradiation mica external detectors were etched in 40% HF for 30 min at $20 \pm 1^\circ\text{C}$. Fission track counting, length measurements of horizontal confined tracks, and apatite composition, based on etch pit size, were determined with a Zeiss Axioplan microscope, equipped with a digitizing tablet and computer driven stage with 1250x magnification using a dry objective. Sample ages were determined using the zeta calibration method and IUGS recommended age standards [Hurford, 1990].

[18] Inclusion-free apatite grains for dating were hand-picked from heavy mineral concentrates previously prepared for AFT determinations. Grain diameters ranged from 80 to 210 μm but grain diameter variation in each aliquot was minimized in order that the standard deviation of the recoil correction was no more than $\pm 0.5\%$. Samples were loaded into platinum microtubes for helium outgassing and U-Th determination. Outgassing was achieved using an induction furnace at a temperature of 950°C . The abundance of ^4He was measured relative to a 99.9% pure ^3He spike in a Pfeiffer Prisma 200 quadrupole mass spectrometer. Measurement of U-Th was conducted on an Agilent 7500a quadrupole mass spectrometer using spiked solutions of the dissolved apatite. Repeated analysis of the California Institute of Technology laboratory Durango apatite standard gives an age of $31.3 \pm 0.2 \text{ Ma}$ (2σ), based on 40 analyses. This error of the mean (6.7%), combined with the U-Th and He analytical uncertainties, was used as a measure of the total uncertainty in sample age. The standard deviation of the

Table 1. Apatite FT Ages of Fully and Partially Reset Samples^a

Sample	Formation/ Deposition Age	Longitude (°E)	Latitude (°N)	Altitude (m)	Number of Grains	ρ_d	Nd	ρ_s	Ns	ρ_i	Ni	P(χ^2)	Re%	Central Age (Ma)
CHA1	Jurassic	51.4	36.5	271	20	1040000	5785	199000	235	1780000	2016	35.6	8.7	20.5 ± 1.5
CHA2	Jurassic	51.3	36.4	532	24	1040000	5766	172000	148	855000	716	72.1	0	35.6 ± 5.1
CHA3	Precambrian	51.2	36.3	1417	16	1040000	5766	138000	109	1140000	865	1.8	38.8	21.7 ± 3.4
CHA4	Jurassic	51.4	36.2	2952	26	1260000	8731	234000	229	1840000	1749	0.1	39.7	26.6 ± 3.0
CHA5	Jurassic	51.3	36.2	2583	12	1260000	8731	42500	17	585000	241	87.7	0	15.0 ± 3.8
CHA6	Cambrian	51.3	36.1	2146	20	1040000	5785	150000	164	1510000	1658	71.6	0	17.4 ± 1.4
CHA7	Eo-Oligocene	51.0	35.9	1525	20	1040000	5785	28100	67	407000	903	29.8	17.5	13.1 ± 1.7
CHA8	Eocene	51.1	35.8	1409	15	1260000	8731	69000	20	630000	212	90.4	7.5	15.2 ± 9.1
FIR1	Cretaceous	53.2	36.4	134	13	1260000	8731	224000	46	714000	149	87.3	0	42.4 ± 23.3
FIR2	Jurassic	53.0	36.2	516	40	1040000	5766	300000	601	424000	805	0	44	130.3 ± 12
FIR3	Jurassic	53.1	36.1	1126	32	1040000	5785	436000	366	2430000	2532	0	78.8	26.4 ± 4.2
FIR4	Cambrian	52.9	35.9	2018	10	1040000	5766	128000	26	1120000	256	64.3	2.8	17.8 ± 3.7
FIR5	Cambrian	53.3	35.8	2290	16	1040000	5766	472000	246	2810000	1422	91.5	0	30.3 ± 2.1
FIR6	Permian	53.3	35.8	2290	9	1040000	5766	133000	43	974000	315	69.5	0.1	23.9 ± 3.9
FIR7	Jurassic	53.3	35.7	1599	19	1040000	5766	216000	112	2020000	1054	13.9	27	18.4 ± 2.2
HAR1	Jurassic	52.4	36.2	612	8	1260000	8731	86200	32	925000	361	0.4	47.8	35.0 ± 10.2
HAR2	Jurassic	52.3	36.0	1377	17	1040000	5766	131000	56	1580000	681	20.3	4.4	14.5 ± 2
HAR3	Jurassic	52.1	35.9	1936	8	1260000	8731	446000	62	1730000	247	61.4	0	53.2 ± 7.6
HAR4	Jurassic	52.5	35.7	2141	11	1040000	5766	128000	32	1340000	356	68.7	1.2	15.8 ± 2.9
HAR5	Neogene	52.1	35.4	1329	17	1260000	8731	147000	107	1100000	798	58.5	33	24.7 ± 6.0
SEF1	Jurassic	49.5	37.0	238	20	1130000	6275	154000	172	1060000	1094	6.1	54.8	35.9 ± 8.9
SEF2	Jurassic	49.4	36.8	239	8	1260000	8731	54800	15	559000	163	82.5	0	19.6 ± 5.3
SEF3	Jurassic	49.7	36.8	1616	21	1260000	8731	89100	75	694000	633	75.7	0	28.8 ± 5.3
SEF4	Eo-Oligocene	49.1	36.6	1811	31	1130000	6275	237000	301	1420000	1836	59.5	4.7	31.3 ± 2.0
SEF5	Eo-Oligocene	49.1	36.6	2422	23	1130000	6275	479000	595	2190000	4454	37.5	15.3	41.0 ± 3.6
SEF6	Eo-Oligocene	48.9	36.5	2009	31	1130000	6275	188000	443	903000	2207	3.2	19.9	38.8 ± 2.5
SEF7	Eo-Oligocene	49.1	36.3	2039	18	1130000	6275	205000	154	997000	746	67.4	1.5	39.4 ± 3.5
SHA1	Pre-Cambrian	50.1	37.2	28	20	1040000	5785	36900	62	629000	1084	37.8	3.4	10.1 ± 1.3
SHA2	Eo-Oligocene	50.0	36.7	1757	20	1040000	5766	113000	143	1240000	1516	66.9	0.8	16.6 ± 1.5
SHA3	Eo-Oligocene	50.0	36.6	1126	20	1040000	5785	151000	126	790000	713	7.9	25	31.7 ± 3.6
SHA4	Jurassic	49.9	36.6	1346	23	1260000	8731	66900	102	429000	665	40.7	6	32.6 ± 3.5
SHA5	Eo-Oligocene	50.0	36.4	1716	5	1040000	5785	113000	27	466000	121	72.7	0	39.2 ± 8.4
TAL1	Cambrian	50.5	36.5	2009	13	1260000	8731	155000	85	1860000	988	19.4	28.1	19.9 ± 6.9
TAL2	Eo-Oligocene	50.4	36.3	2212	21	1260000	8731	30400	49	355000	620	100	0	16.5 ± 3.3
TAL3	Jurassic	50.5	36.9	1790	7	1040000	5766	266000	42	2810000	450	93.1	0	16.4 ± 2.7
GOR1	Neogene	53.9	36.6	1109	19	1040000	5766	554000	345	1350000	876	0	47.9	66.6 ± 8.9
GOR2	Neogene	53.9	36.5	1731	32	1150000	7934	215000	191	679000	738	0	67	70.2 ± 17.5
TEH1	Neogene	51.9	36.5	14	14	1040000	5766	187000	132	1210000	848	0	69.4	29.4 ± 6.4
TEH2	Neogene	51.9	36.5	92	4	1040000	5785	108000	14	888000	115	72.16	0	21.4 ± 6.1
TEH3	Cretaceous	51.9	36.5	427	14	1040000	5766	211000	77	462000	170	50.4	1.8	79.4 ± 10.9
TEH4	Jurassic	51.7	36.4	1430	16	1260000	8731	1980000	717	2370000	887	35.9	26.2	157.4 ± 24
TEH5	Jurassic	51.9	36.2	1799	13	1260000	8731	188000	43	2190000	493	90.0	0	18.5 ± 3.0
TEH6	Eo-Oligocene	51.8	35.8	2294	3	1040000	5785	190000	11	1190000	65	82.7	0	29.8 ± 9.7
TEH7	Paleocene	51.8	35.8	2110	27	1260000	8731	109000	114	656000	690	89.3	0.3	35.1 ± 3.6
TEH8	Eocene	51.6	35.7	1491	8	1470000	8167	276000	74	2170000	585	34.4	14.4	31.8 ± 4.3
TEH8	Eocene	51.9	36.5	1491	7	1040000	5785	237000	44	1360000	240	37.4	1.1	32.2 ± 5.3

^aNote that ρ_d , ρ_s and ρ_i represent the dosimeter, sample spontaneous and induced track densities ($\times 10^6$ tracks cm^{-2}); P(χ^2) is the probability of χ^2 for n degrees of freedom where n = no. of crystals⁻¹. All ages are central ages [Galbraith and Laslett, 1993].

age replicates (typically 3–4) was used as the error when it exceeded the analytical uncertainty. Reported He ages have been corrected for alpha ejection effects based on measured grain dimensions [Farley *et al.*, 1996] using the procedure of Gautheron *et al.* [2006].

[19] Table 1 provides a summary of the AFT data. In general the sampled rocks had low abundances of apatite, many with low uranium concentration. These factors inevitably impacted on data quality, especially track length measurements. The low number of apatites and their general poor quality also confined (U-Th)/He age determination to 10% of the FT dated samples. Nevertheless, good quality data sets suitable for thermal history modeling (>50–100 track lengths and >15–20 single grain ages) were obtained for samples representative of the range of AFT ages e.g., from 16.6 ± 1.5 Ma (SHA 2, Eocene intrusive), to $157.4 \pm$

24 Ma (TEH 4, Jurassic sedimentary rock). Fully or partially reset samples (AFT age < stratigraphic age) are from pre-Neogene rocks, while un-reset samples are from rocks that are Neogene in age. The majority of the reset samples yielded AFT central ages of between 10 Ma and 40 Ma, only six samples had central ages over 40 Ma. Four partially reset samples (TEH 3, TEH 4, FIR 1, and FIR 2) show over-dispersion of single grain ages some of which are older than the stratigraphic age of the sampled formation. Consequently, the bulk of samples record cooling linked to growth of the Alborz orogen.

[20] Table 2 lists the AHe results. Good AHe data were measured on samples SEF 4 and SEF 5 from a pluton in the southwestern Alborz, CHA 1 from the central north Alborz, and TAL 2 from a granitoid body in the mountain range to the south of the Shah Rud valley. These data were

Table 2. Apatite (U-Th)/He Ages Performed by Furnace Heating for He Extraction and ICP-MS for U-Th Determinations at the University and Birkbeck College of London^a

Aliquot Number	n	He nmol/g	U (ppm)	Th (ppm)	FT	He age (Ma)	Error	Standard Deviation
<i>Sample TAL2</i>								
A	3	0.48	4.59	20.41	0.80	11.7	0.7	
E	3	0.53	5.02	26.53	0.77	11.3	0.7	
F	3	0.47	4.12	19.69	0.83	11.9	0.7	
Mean		0.49	4.58	22.21	0.80	11.6	0.4	0.3
<i>Sample CHA1</i>								
A	2	0.71	20.03	31.17	0.84	5.7	0.3	
B	4	0.63	19.42	20.28	0.79	6.1	0.4	
D	3	0.31	8.08	24.66	0.78	5.3	0.3	
E	4	1.15	39.04	43.04	0.78	5.5	0.3	
Mean		0.70	21.64	29.79	0.80	5.6	0.2	0.3
<i>Sample SEF5</i>								
A	2	4.70	25.46	83.23	0.79	15.8	0.9	
B	3	0.03	0.14	0.48	0.73	16.8	1.0	
C	2	3.82	34.94	57.84	0.75	19.4	1.2	
Mean		2.85	20.18	47.19	0.75	17.3	0.6	1.9
<i>Sample SEF4</i>								
A	3	0.95	12.06	30.37	0.77	11.8	0.7	
B	2	1.16	26.56	54.93	0.73	7.4	0.4	
D	3	1.07	16.93	30.57	0.74	10.9	0.7	
Mean		1.06	18.52	38.62	0.75	10.1	0.4	2.3

^aThe estimated analytical uncertainty for He ages is about 6% (2σ). The standard deviation is used as the error when it is greater than the analytical uncertainty. Aliquots were not used for the calculation of the average age.

interpreted alongside results from previous studies listed in Table 3 [Axen *et al.*, 2001a, 2001b; Guest *et al.*, 2006b].

[21] To define rock exhumation histories, selected good quality data were modeled to determine probable thermal histories using HeFTy software [Ketcham, 2005], incorporating a multikinetic fission track annealing model [Ketcham *et al.*, 2007] and a He diffusion model [Farley, 2000] for Helium data. Joint modeling of AFT and AHe data was only possible for sample SEF 5 as the other samples were limited by lack of track length data. Where appropriate, geological constraints (intrusion or volcanic age, depositional ages), were also incorporated into the modeling.

4. Interpretation

[22] Comparison of AFT age and sample elevation for all data covering both flanks provides a useful way to examine how rock uplift is distributed across the range. Figures 6a

and 6b show age-elevation relationships, distinguishing between data from the north and south flank of the mountain range, for the entire data set (6a), and for only those samples that have been fully reset (6b). No age-elevation correlation is apparent at this scale but there are noticeable groupings of AFT ages of circa 10–20 Ma (Middle Miocene), 30–35 and 35–45 Ma (Eocene-Oligocene transition). These groups are found across the entire elevation range, indicating kilometer scale exhumation during these time intervals. A fourth grouping involves older ages that tend to increase with elevation, consistent with much slower rates of burial and exhumation. Notably, there is a contrast between the north flank, with a large spread in AFT ages from 10 Ma to 157 Ma, and the south flank with exclusively Cenozoic AFT ages.

[23] It is also useful to distinguish between data from the fringes of the mountain belt, with limited relief, and the zone around the main divide, where elevation and relief are

Table 3. Published AHe Ages for the Alborz

Author	Sample Number	U-Th-He Age (Ma)
This study	1(SEF4)	10.1 ± 0.4
	2(SEF5)	17.3 ± 0.6
	3 (TAL2)	11.6 ± 0.4
	4 (CHA1)	5.6 ± 0.2
Guest <i>et al.</i> [2006b]	5	13.3 ± 0.7; 16.1 ± 0.8; 17.2 ± 0.9
	9	3.4 ± 0.2; 4.2 ± 0.2; 4.7 ± 0.2; 5.8 ± 0.3; 6.1 ± 0.3
	10	5.1 ± 0.3; 6.9 ± 0.3
	11	4.0 ± 0.2; 4.3 ± 0.2; 4.8 ± 0.2; 5.8 ± 0.3; 6.5 ± 0.3
Axen <i>et al.</i> [2001a]	7	5.8 ± 0.3; 8.1 ± 0.7
	8	4.4 ± 0.2; 5.9 ± 0.3
Axen <i>et al.</i> [2001b]	6	6.7 ± 0.3; 5.3 ± 0.3; 4.8 ± 0.2; 3.8 ± 0.2; 6.6 ± 0.3; 5.2 ± 0.3; 4.1 ± 0.2; 2.8 ± 0.1
	12	11.3

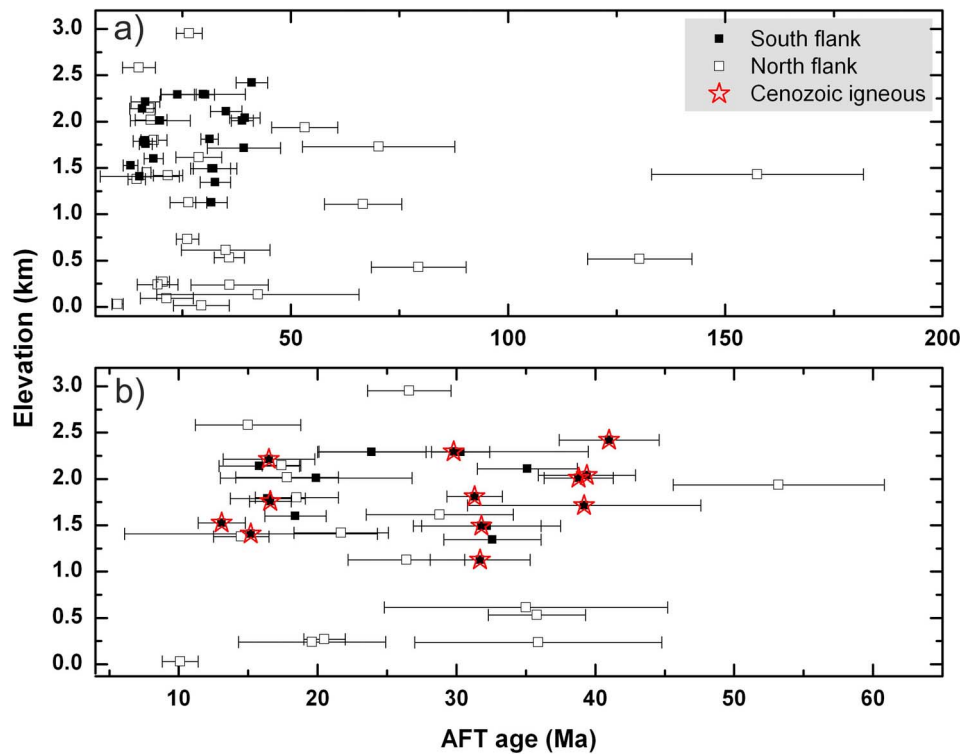


Figure 6. Plot of AFT age against elevation for (a) all sampled rocks including partially and fully reset and (b) only fully reset. Differentiation between north-south flanks has been done using open-and black rectangles, respectively. Cenozoic igneous rocks are displayed as red stars.

greatest. Examination of the data in this way shows an anti-correlation between AFT ages and elevation in the axial zone of the mountain belt, but not along exterior profiles (Figure 7). The anti-correlation may have been caused by systematically higher rates of exhumation in areas with high elevation, decreasing relief of the range on the AFT time scale, or the role of paleo-topography in which the modern valleys are in approximately the same positions as they were at the beginning of the exhumation [e.g., House *et al.*, 1998; Reiners, 2007]. Although other explanations cannot be excluded with the data at hand, the broad spatial pattern of AFT cooling ages suggests that gradients in exhumation rate are likely to be responsible for the anti-correlation of cooling age and elevation in the axial part of the mountain belt. In this explanation, the pairing of high elevation with young cooling age can only be achieved if the highest topography has formed in the areas with the highest rock uplift rates. In the next sections we examine the data to discern which samples have been buried sufficiently to reset the apatite thermochronometers and then consider the spatial distribution of the reset and un-reset AFT and AHe ages along eight transects, oriented perpendicular to the strike of the mountain belt.

4.1. Un-reset and Partially Reset Samples

[24] Sandstones that have not been buried to any significant (>1–2 km) depth will likely retain a strong provenance signal and therefore provide an opportunity to prospect for earlier exhumation events subsequently obscured in the

orogen, and to constrain regional depths of erosion. While the most recently deposited sandstones are likely to have experienced the least reburial and reheating, older sedimentary rocks deposited at the fringes of the mountain range may also have experienced minor levels of burial permitting this approach. Un-reset samples have single grain AFT ages that are all older than the host sedimentary rock deposition age. By contrast partially reset samples (caused by heating due to burial beneath at least 1–2km of cover rocks) contain a range of single grain ages that reflects variable levels of fission track annealing due to differences in apatite composition (imposed by the apatite provenance). This results in some grain ages that are older than sample depositional age (most resistant apatites, typically rich in chlorine), and other grains that have been totally reset (least resistant, fluorapatite compositions).

[25] Un-reset characteristics were found in Neogene sandstone samples, GOR1, GOR2, HAR5, TEH1, and TEH2. Samples GOR 1 and GOR 2 from the easternmost Alborz have central FT ages of 66.6 ± 8.9 Ma and 70.2 ± 17.5 Ma, respectively, both significantly older than the depositional age of the sediments (stratigraphic age of Middle-Late Miocene ca. 5.3–16 Ma). Over-dispersion of the single grain ages in these samples signifies a mixed population of ages that can be deconvolved into source age components using a binomial peak-fitting method [Galbraith and Green, 1990]. Decomposition reveals two principal age populations (Figure 8) belonging to the Late Paleozoic (15% of grains at 293 Ma) and Early Paleogene (85% of grains at

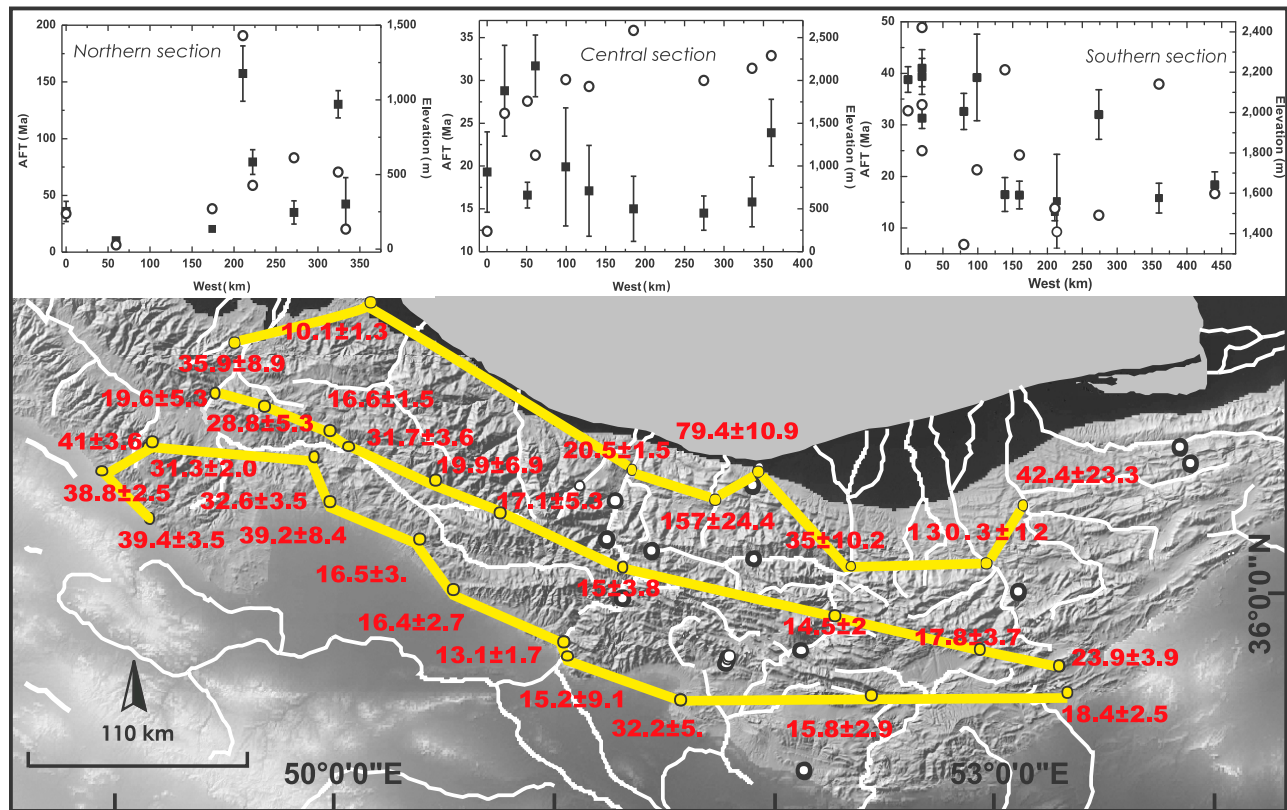


Figure 7. Longitudinal AFT age-topographic elevation in cross sections through northern, central and southern Alborz (left to right, respectively). Sample locations (yellow circles) are placed on a SRTM sourced topography of the Alborz. Elevation and AFT central ages ($\pm 1 \sigma$) are displayed in white circles and black rectangles, respectively.

50 Ma). Pliocene rocks sampled on the northernmost edge of the central part of the mountain range (TEH 1 and TEH 2) have also recorded a provenance exhumation history, but in this case most grains belong to a younger age population around 24 Ma. Without track length data for this population we cannot be certain if this age relates to fast or slow cooling but given that this was a time of relative tectonic quiescence the latter scenario is the more likely. HAR5 from the southern fringe of the mountain belt has central AFT ages of 24.7 ± 6 , that is older than the depositional age of the sediments (Middle-Late Miocene: ca. 5.3–16 Ma). Decomposition of the single grain ages reveals the principal age population belonging to the Eo-Oligocene (89% of grains at 31.6 Ma).

[26] Four samples (FIR 1 and FIR 2, and TEH 3 and TEH 4) have evidence of partial resetting. These were collected from Cretaceous and Jurassic sedimentary rocks in the northeast of the mountain belt, the same area that has yielded most of the un-reset samples. Jurassic sandstone FIR 2 has a central FT age of 130.3 ± 12 Ma with over-dispersion (relative error 44%) relating, in part, to a minor sub-population of reset grains, as shown by the radial plot in Figure 8. These youngest grains were reset by peak post-burial temperatures and therefore approximate to the time of onset of magmatic cooling, ca. 43 Ma.

[27] The partially reset samples sit structurally well within the zone of mountain building, close to the North Alborz and Khazar faults. Similarly, the five un-reset samples collected from the central and eastern segments of the Alborz

Mountains were collected inside the zone of active mountain building (Figure 5). The implication is that either this zone has expanded since deposition of the samples, or alternatively the sedimentary rocks have been advected into it by sub horizontal tectonic transport. Given that a paleohigh may have existed since the Middle Mesozoic in the north Alborz [Sussli, 1976; Salehi Rad, 1979], we attribute the partially reset ages to erosion of a proto-Alborz topography. To assess the alternative assumption, we have plotted (Figure 9) AFT ages along the northern boundary and compared these with corresponding values of dip-slip and strike-slip rates obtained from published GPS records [Djamour et al., 2010]. This longitudinal section corresponds to the northern section shown in Figure 7. Plotted ages are central ages for fully reset and partially reset samples. An anti-correlation between present dip-slip rate and AFT ages provides an explanation for the increase in AFT ages toward the east and the patch of partially reset Mesozoic bedrock samples in the NE of the northern Alborz. This suggests that the current kinematic regime and pattern of deformation existed in the geological past, at least for the northern Alborz and implies long-lived vertical motion with variation along the Khazar Fault. Stratigraphic records are consistent with the short-term kinematics. In the few locations where Pliocene sedimentary rocks are found in outcrop, they occur at ~ 1000 m above sea level and only south of the Khazar Fault. Pliocene rocks north of the fault are only found in exploration wells in the South Caspian Basin

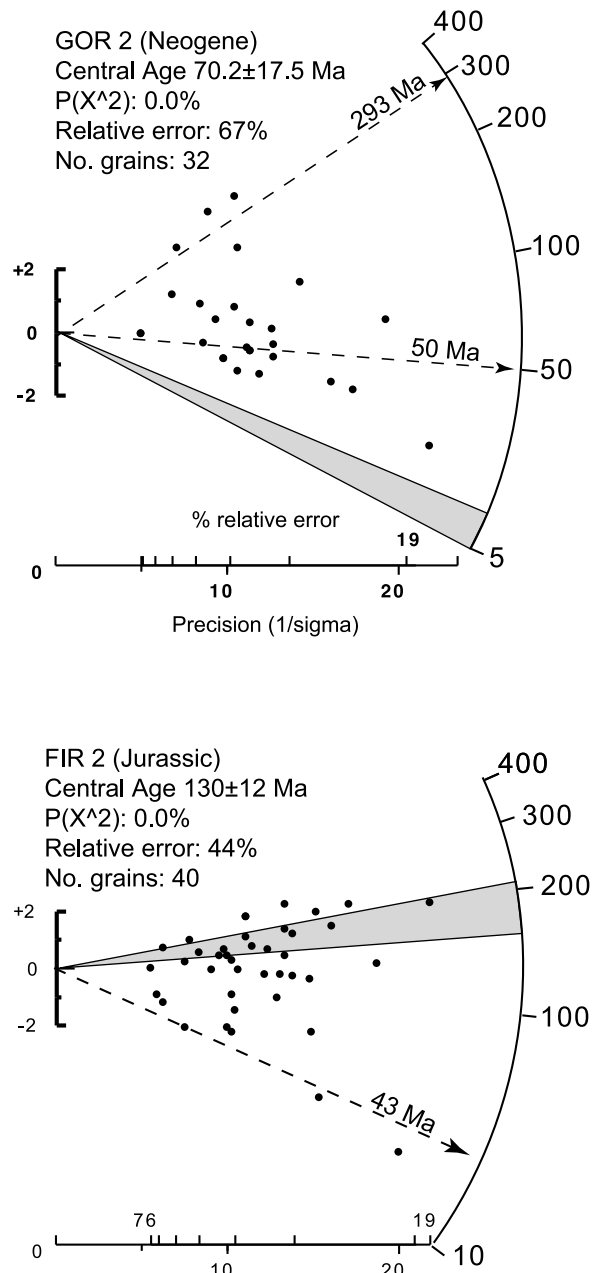


Figure 8. Radial plots showing examples of the distribution of single grain ages for un-reset sample GOR2 and partial reset samples FIR2. The shaded region on the radial plots represents sample deposition age. The age components (dashed lines) were extracted using binomfit [Brandon, 1992].

beneath 1600–2000 m of Quaternary sediments, indicating rapid basin subsidence [Berberian, 1983]. The subsidence rate dramatically increases from east to west and from onshore to offshore [Yassini, 1981].

[28] Sample FIR 2 was collected in the immediate hanging wall of the North Alborz Fault (south of the Khazar Fault in the northern mountain front) (Figures 3 and 5): the vertical offset on the eastern segment of that fault may not have been more than a few kilometers, which is in contrast with the segment toward the west (Chalus section) where data from

sample CHA1 indicates at least 4–5 km of vertical offset on the North Alborz Fault since the earliest Miocene. Recent GPS measurement shows that the North Alborz Fault and other faults in the NE Alborz have major strike-slip, which has been argued to be a relatively recent attribute [Djamour *et al.*, 2010]. The low levels of fission track annealing recorded by the AFT data from the NE Alborz reflect lower levels of exhumation than elsewhere in the mountain belt and this would fit with most of the deformation by strike-slip faulting. How far this zone of limited exhumation extends is not well defined. Lack of un-reset AFT ages in rocks further west along the northern margin of the mountain belt may be due to a lack of Neogene samples from this area. However, presence of fully reset AFT ages from the same stratigraphic units in the West Alborz, implies that early uplift of the proto-Alborz did not extend further to the west. By contrast all samples from the south margin of the Alborz, with the exception of the southernmost sample, HAR5 (with stratigraphic age of Neogene), have been reset, implying that exhumation in that area has been substantial even at the topographic edge of the mountain belt.

4.2. Reset Samples and Postmagmatic Emplacement Ages

[29] In the majority of cases AFT central ages from pre-Tertiary and Paleogene rocks fall between 10 Ma and 40 Ma, only 6 samples are older than 40 Ma. Sampled pre-Tertiary rocks include Paleozoic-Precambrian units but most samples are from the Shemshak Formation (depositional age range ~210–160 Ma). Paleogene samples are mainly igneous rocks (formation ages from 65 to 23 Ma in Figure 4). Thus in most cases the fission track data record Cenozoic exhumation. Most of these samples fall into one of three broad age categories, according to their AFT age distribution:

[30] 1. Middle Eocene cooling ages are limited to the southwest Alborz, specifically the Tarom Range and the mountains northwest of Qazvin (Figure 3) where Eocene magmatic rocks are the principal substrate. AFT ages in

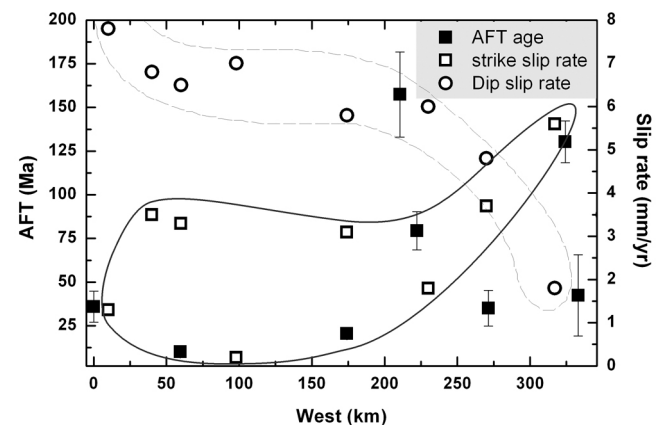


Figure 9. Longitudinal AFT age-slip rates on a cross-section through the South Caspian shoreline. The variation of AFT ages along the northern boundary is compared with counterpart values of dip-slip and strike-slip rates modeled by GPS records [Djamour *et al.*, 2010]. Polygons have been drawn around to help distinguish the anti-correlation and correlation fields.

these rocks are likely associated with magmatic cooling, and indicate that later exhumation has been limited.

[31] 2. Cooling ages around the Eocene-Oligocene transition were found in rocks flanking the cluster of Middle Eocene ages, implying that early exhumation of the western Alborz occurred mainly to the north and east of the area of Eocene magmatic activity. Another grouping of samples with AFT ages from this first phase of exhumational cooling is located near Tehran, and includes the un-reset sample HAR 5 (the principal age population belonging to the Eo-Oligocene).

[32] This group may be bounded to the west by the North Tehran Fault, but extends north across the Moshfa Fault. Importantly, both groups are confined mainly within areas with little topography above 2 km, and relief <500 m. Isolated samples with ages around 32 Ma outside these two groups are all located outside the highest mountain areas.

[33] 3. Samples, from the high mountains of the central Alborz generally have AFT ages associated with Middle Miocene exhumational cooling. Between Karaj and Qazvin, this domain extends to the southern fringe of the mountain belt, and it is apparent that in this area there has not been a major outward migration of the deformation front in the recent geological past. Notably, most of the youngest AFT ages were found to the south of the Kandavan-Baijan-Banan-Rudbar fault array, which also defines the boundary between domains dominated by Tertiary rocks to the south and pre-Tertiary rocks to the north. A similar pattern is also found along the E-W Moshfa-Taleqan fault array further east. These arrays may be long-lived structures that have controlled the region's kinematics throughout the Tertiary [Yassaghi and Madanipour, 2008].

4.3. Transects

[34] Some details of the AFT age pattern are best viewed along sections across the mountain belt. Figure 5 shows swath profiles (with ~20 km width) of mean, minimum and maximum topographic elevations for each of the eight N-S sections together with major faults, sampled locations, and AFT and stratigraphic ages. Salient details are reviewed from east to west.

[35] The Firuzkuh section in the eastern Alborz shows the domain of partially reset rocks with old cooling ages extending into the hanging wall of the North Alborz Fault. This domain appears to terminate abruptly between sites FIR 2 (130.3 ± 12 Ma) and FIR 3 (26.4 ± 4.2 Ma). Ten kilometers separate these two sites, and it is likely that a structure with a large amount of dip slip is located in between. This structure has not yet been identified in outcrop. Further south, AFT ages are uniformly young, where data are available, and indicate kilometer scale exhumation since the Miocene e.g., FIR4 (17.8 ± 3.7 Ma) and FIR7 (18.4 ± 2.2 Ma) collected from the hanging walls of the Firuzkuh and Diktash faults.

[36] At the northern end of the Haraz section, HAR 1 (35.0 ± 10.2 Ma) is fully reset but its AFT age and the large dispersion of single grain ages indicate that slow exhumation of the NE Alborz extends into this section. As in the Firuzkuh section, there is a significant jump to younger cooling ages within the north flank of the mountain belt toward the divide (e.g., HAR 2- 14.5 ± 2.0 Ma). HAR4 (15.8 ± 2.9 Ma), in the hanging wall of

Moshfa Fault, indicates kilometer scale vertical offset since the Early Miocene.

[37] The partially reset domain of the NE Alborz is again picked up in the Tehran section (un-reset Neogene samples TEH 1 and TEH 2 and partially reset Cretaceous sample TEH 3), where Jurassic sample TEH 4 (157.4 ± 24.4 Ma), from the hanging wall of the North Alborz Fault, has not been totally reset. Fully reset rocks have only been recovered from locations south of the Kojour Fault. This structure may extend significantly further east to explain the jump in AFT ages toward the divide observed in the Firuzkuh and Haraz sections. Three locations with AFT ages close to the Eocene-Oligocene transition in the south flank of the mountain belt are all to the south of the Moshfa Fault, which may therefore form the southern boundary of the fast exhuming, high interior of the Alborz Mountains. This active fault has a left-lateral nature. Detailed structural analysis indicates that the central part of the Moshfa Fault is an inverted normal fault, which has been reactivated as a reverse fault since the late Tertiary [Moinabadi and Yassaghi, 2007].

[38] In the Chalus section, the relatively young AFT age of CHA 1 (20.5 ± 1.5 Ma) indicates kilometer scale vertical offset on the North Alborz Fault since the earliest Miocene. However, the Kandavan Fault, located almost on the main divide of the mountain belt, appears to be the northern limit of a domain with uniform, high exhumation rates, reflected in Miocene AFT ages. It has been identified as an inverted basin-bounding fault, that controls development of the Eocene rocks in its footwall [Yassaghi and Naeimi, 2011]. Along this section, the North Tehran Fault has stepped out to the southern front of the mountain belt, and it has taken over from the Moshfa Fault as the main structure bounding the domain with youngest AFT ages to the south. The youngest AFT ages in this section, e.g., CHA8 (13.1 ± 1.7 Ma), are consistent with rapid exhumation since the Middle Miocene. The zone of rapid exhumation extends west into the Taleqan section along the south flank of the mountain belt (Figure 5). No samples from north of the Kandavan Fault are available in this section and the local role of this fault, as a bounding structure cannot be assessed. As in the Tehran section, the southern boundary of the domain with Miocene AFT ages appears to be located at the mountain front, here defined by the Moshfa and Takieh faults.

[39] The Shah Rud section represents a dramatic break from the trends observed further east. In this section, relatively old, Eocene AFT ages are found in the south, associated with Tertiary plutonic rocks. In the north flank of the Shah Rud valley, a sharp decrease in AFT age toward the north over a short distance may signal offset along a major structure, which could well be the Kandavan Fault. However, in contrast to sections further east, it is the northern block that has been exhumed fastest. Sample SHA 1 (AFT age 10.1 ± 1.3 Ma), at the northern edge of the mountain belt, has the youngest of all AFT ages in this study, but notably, rapid exhumation of this Neoproterozoic granite (Lahijan granite), with a zircon U-Pb age 551 ± 9 Ma [Guest *et al.*, 2006b], has not resulted in the construction of a major topographic feature. The Lahijan granite is located on the hanging wall of the Khazar Fault, where the shortening component recorded by GPS is among the highest along the fault [Djamour *et al.*, 2010].

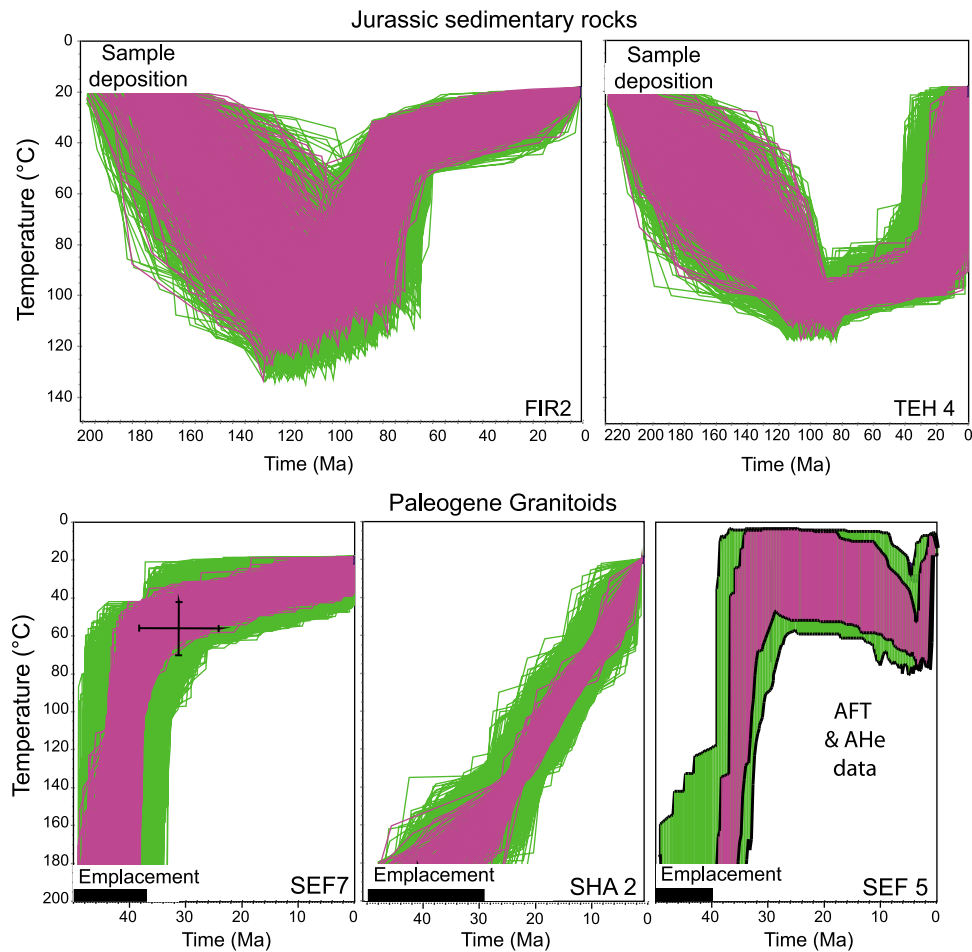


Figure 10. Examples of thermal history models for Jurassic sedimentary rocks and Paleogene granitoids. Sample SEF 5 included both AFT and AHe data. Modeling used HeFty software [Ketcham, 2005] incorporating a multikinetic fission track annealing model [Ketcham *et al.*, 2007] and a He diffusion model [Farley, 2000] for Helium data. DPAR was used as a compositional proxy. Time-temperature constraints were used for sample depositional age or rock formation age, otherwise the models were allowed unconstrained search space. For sample FIR 2 the thermal history is related to the older age component only from which the track length data were obtained.

[40] Finally, the Sefid Rud section repeats the pattern of the Shah Rud section to the east, with Middle Eocene AFT ages in the south, and a jump to Neogene ages along the topographic depression carved out by the river's trunk stream. The age difference between SEF 2 (19.6 ± 5.3 Ma) and SEF 3 (28.8 ± 5.3 Ma) may be due in part to the 1.5 km difference in elevation between these two samples. However, SEF 1 is from a low elevation (238m) and its Eocene age must reflect a return to slow exhumation of the northern mountain front.

[41] The trends outlined above have not extended into our AHe results and previously published AHe data. Previous AHe studies of exhumational cooling have focused on the Tehran, Karaj-Chalus, and Alam Kuh areas, covering a limited part of the central-west Alborz [Axen *et al.*, 2001a, 2001b; Guest *et al.*, 2006b]. In addition, Davidson *et al.* [2004] have published a series of AHe ages of lava flows associated with the Damavand eruptive center but these have not been included here as they are unrelated to the exhumation history of the Alborz. All published ages are shown

in Table 3 with geographic location (red stars) in Figure 3. Most AHe ages cluster between 3 and 6 Ma, indicating cooling from ≥ 60 – 80°C over this period. Older ages up to 17 Ma have been found, but their significance is unclear due to lack of agreement with AFT data. For example, Guest *et al.* [2006b] obtained AHe ages of 17.2–13.3 Ma for a Late Precambrian granite body (U/Pb age 551 ± 9 Ma) located near Lahijan on the SW Caspian coast. These ages are older than the AFT age (10.1 ± 1.3 Ma) we have obtained for the same body (SHA1). The granite complex is large, with considerable relief. It is possible that differential exhumation may explain this disparity or, alternatively, technical issues may be the cause. In any case, (U-Th)/He ages of 162–133 Ma for zircons from the same location [Guest *et al.*, 2006b] appear to limit the Neogene exhumation to little more than the depth of the AFT partial annealing zone (broadly, ≤ 110 – 120°C).

[42] The utility of complimentary AFT and AHe data is demonstrated by the 17.3 ± 0.6 Ma AHe age obtained by this study for Paleogene granitoid sample SEF 5, which has

an AFT age of 41.0 ± 3.6 Ma. When jointly modeled these two sets of data show rapid cooling to (near-) surface temperatures in the Eocene followed by reburial to depths sufficient to partially reset the AHe system. Subsequent inversion and exhumation were recent and took place at or after 5 Ma (Figure 10), which is consistent with the main cluster of young AHe ages. Four AHe dates for Eocene volcanics and Neogene detrital rocks in the uppermost Shah Rud catchment are between 3.4 ± 0.2 Ma and 6.1 ± 0.3 Ma [Guest *et al.*, 2006b]. Seven further AHe dates for Paleozoic, Mesozoic and Eocene rocks from several locations N-NW of Tehran record cooling to below 40–70°C between 4.0 ± 0.2 Ma and 6.5 ± 0.3 Ma [Guest *et al.*, 2006b]. Eocene rocks of the Karaj Formation above an active thrust with Pliocene-Pleistocene footwall strata in the area north of Tehran have an AHe age of ~ 11.3 Ma [Axen *et al.*, 2001b].

5. Discussion

[43] Combination of thermochronometric and stratigraphic data provides the fullest picture of the evolution of the Alborz mountains. Rock uplift and denudation associated with development of the Alborz Mountain belt were not constant through time and several episodes of tectonic movement spanning the Cretaceous-Paleocene, Eocene-Oligocene, Middle Miocene and Miocene-Pliocene have been proposed [Ballato *et al.*, 2011; Berberian and King, 1981; Axen *et al.*, 2001a; Allen *et al.*, 2003; Guest *et al.*, 2006b]. With constraints provided by thermochronometry data we can now identify key stages in the development of the Alborz Mountains and assess their cause and significance.

5.1. Late Cretaceous Compression and Emergence

[44] A Late Cretaceous-Early Paleocene unconformity extends beyond the southern Alborz, throughout the greater part of central Iran. It is overlain by the Fajan conglomerate which is interpreted to reflect compression and uplift of much of the Iranian Plateau, including the Alborz [Berberian and King, 1981; Berberian, 1983; Ziegler, 2001] during the closure of some small oceanic basins further south in Iran, now preserved as Late Cretaceous ophiolite complexes. This early phase of shortening across Iran substantially pre-dates initial Arabia-Eurasia collision [Brunet and Cloetingh, 2003]. Instead, it is likely to reflect the relative movement of smaller plates north of the main Neo-Tethys, which was undergoing northward subduction under Eurasia at the time.

[45] A proto-Alborz Range had emerged by the Early Tertiary [e.g., Stöcklin, 1968; Clark *et al.*, 1975; Sussli, 1976; Berberian, 1983]. In fact, some workers have suggested that subaerial topography may have existed in the northern Alborz as early as the Middle Mesozoic [Sussli, 1976; Salehi Rad, 1979], as discussed in section 4–1, and our thermochronometric data appears to confirm this. This topographic barrier would have separated the South Caspian Basin from central Iran [Stöcklin, 1968]. It may have been delimited by the precursor of the Khazar and South Talesh faults [Berberian, 1983] to the north, and an array of faults bordering the Mid-Eocene volcanics, aligned with the present Kandavan fault system to the south. While the southern Alborz was transgressed after the Early Paleocene, the northern Alborz may have remained a subaerial landmass throughout the Paleogene [Sussli, 1976; Huber, 1977]. This

is supported by lower levels of fission track annealing in the un-reset and partially reset samples from the NE compared to elsewhere in the mountain belt.

5.2. Middle Eocene Magmatism

[46] The stratigraphy of the southern Alborz reflects a return to marine conditions in the Paleocene, persisting throughout the Eocene. The deposits have a significant volcanoclastic component, from sources located within north Iran. The Middle Eocene was punctuated by the intrusion of plutons including the Tarom, Lavasan, and Qasr-e-Firuzeh intrusions with emplacement ages of 35–40 Ma [Davari, 1987; Rezaeian, 2008; Ballato *et al.*, 2011]. Magmatic activity appears to have commenced earlier, ~ 40 –50 Ma [Verdel *et al.*, 2011; Ballato *et al.*, 2011], with widest distribution in the Tarom and southern Talesh mountains of the western Alborz [Stöcklin and Eftekhari-Nezhad, 1969; Stöcklin, 1972]. It lasted until 36.0 ± 0.2 Ma [Ballato *et al.*, 2011] and decreased in extent toward the east. There is close agreement between magmatic rock formation ages determined by U-Pb dating [Verdel, 2008] and AFT ages, e.g., SEF 5 in the Tarom intrusion, consistent with emplacement at high levels in the crust. Eocene magmatism was accompanied by extension and subsidence across the southern Alborz, which created accommodation space for several kilometers of volcanic and volcanogenic sediments of the Karaj Formation. The thickness of this formation appears to decrease abruptly along the main divide of the Alborz Mountains and thermochronometric data from the northern Alborz indicate that a thick cover of Cenozoic sediments has not existed there at any time. This constrains the extent of the Eocene basin, and implies that during Eocene extension the proto-Kandavan Fault has been active as a normal fault system with significant topographic relief; the geological evidence also support the normal fault kinematics [Yassaghi and Naemi, 2011]. Eocene extension and magmatism reached beyond the southern Alborz in north Iran, affecting much of the region now occupied by the Pontides, Caucasus, Talesh and Iran Plateau. This region was located in the back arc of an active margin further south, with northward subduction of Neo-Tethys ocean crust [Berberian and King, 1981]. High rates of extension and magmatism in the Middle Eocene have been attributed to rollback of the subducting slab [Vincent *et al.*, 2005].

5.3. Eocene-Oligocene Boundary: Collision, Compression and Mountain Building

[47] In the southern Alborz, Eocene marine and marginal marine deposits of the Karaj and Kond Formations are cut by an erosional unconformity, overlain by a basal conglomerate, continental red beds of the Lower Red Formation, and subaerial volcanics. This is clear evidence of emergence and subaerial exposure of the Alborz region, and substantial sediment supply from the north. The AFT age and elevation plot (Figure 6a) shows that most ages, especially for the south flank, cluster between 20 and 40 Ma across the elevation range, reflecting rapid exhumational cooling at that time. The intensity and geographic extent of erosion in the Alborz region around the Eocene-Oligocene transition, and the proximal nature and lateral extent of the associated sediments indicate the formation of subaerial topography along the arch of the mountain belt, where this signal has not

been overprinted by younger exhumational events. To discriminate between magmatic and exhumational cooling AFT ages have been plotted for the Eocene igneous rocks (Figure 6b). Given that the uppermost (youngest) Eocene tuff in the southern central Alborz has been dated to 36.0 ± 0.2 Ma [Ballato *et al.*, 2011], younger cooling ages must relate to a post-formation thermal history.

[48] Compression in the Alborz in the Late Eocene may have been caused by the onset of collision along the Bitlis-Zagros suture in the Turkish-Iranian Plateau [e.g., Hessami *et al.*, 2001; Haq and Al-Qahtani, 2005; Vincent *et al.*, 2005; Hatzfeld and Molnar, 2010], after the last substantial piece of oceanic plate separating Arabia from Eurasia had been subducted [Allen and Armstrong, 2008]. Following the collision, ongoing convergence between the two plates resulted in compressional deformation of the continental lithosphere, involving folding and thrusting and the construction of mountain belts across the collision zone including the Alborz, Zagros [Ballato *et al.*, 2011; Agard *et al.*, 2005; Hatzfeld and Molnar, 2010], Caucasus [Vincent *et al.*, 2007] and Talesh Mountains [Brunet *et al.*, 2003; Vincent *et al.*, 2005].

5.4. Middle Miocene: Accelerated Exhumation

[49] On the southern fringes of the mountain belt and further south in the Iran interior a shallow marine carbonate shelf (Qom Formation) formed with limited clastic input from surrounding highs. However, in the Middle Miocene (~16–11 Ma), the northern edge of the Qom shelf became subaerially exposed, eroded, and covered by basal conglomerates of the Upper Red Formation that extended far into the basin [Reuter *et al.*, 2009]. The timing for the initiation of Upper Red sedimentation may not have been coeval across the orogen, although Ballato *et al.* [2008] document 17.5 Ma in the southern Alborz mountains, while Morley *et al.* [2009] suggest ca. 17 Ma for central Iran (Qom area).

[50] The source of these conglomerates was located in the Alborz Mountains, where intramontane basins formed and filled with lacustrine, evaporitic and terrestrial deposits. Rapid exhumation of the Alborz Mountains at this time is captured by a strong cluster of AFT ages of 10–20 Ma (Figure 6b), located mainly in the south flank of the central Alborz, and along the main divide of the central and western part of the mountain belt. Throughout this time, the northern edge of the mountain belt was defined by motion on the North Alborz Fault. Neogene formations with Para-Tethyan facies do not crop out south of the North Alborz Fault and the Red Marl Formation (Middle Miocene - Langhian) [Stöcklin, 1972] was deposited unconformably on top of the Late Cretaceous or Early Paleocene strata, indicating an erosion phase or hiatus before onset of marine deposition in the Late Miocene [Yassini, 1981].

[51] The Middle Miocene acceleration of exhumation and sedimentation rates in the Alborz Mountains followed an apparent decrease of the rate of convergence between Arabia and Eurasia from ~3 cm/yr to ~2 cm/yr around 20 Ma, but allowing for the generally low temporal-spatial resolution of the current convergence rate data it is likely that convergence rates have not changed to any great extent since 50 Ma [McQuarrie *et al.*, 2003; Hatzfeld and Molnar, 2010].

5.5. Pliocene-Quaternary: Accelerated Exhumation, Again

[52] The absence of a substantial number of AFT ages younger than 10 Ma is due entirely to the relatively slow pace of shortening and shallow depths of exhumation across the Alborz Mountains after this time. However, the AHe thermochronometer, which has a lower closure temperature than the AFT system and sensitivity to smaller-scale exhumation, has revealed a distinct cooling phase that initiated around 4–6 Ma, which appears to be separated from the earlier, Middle Miocene cooling phase by an interval of slower exhumation in the Late Miocene. The regional stratigraphy records an erosional unconformity (or facies change from fine to coarse clastics) and tectonic tilting [Ballato *et al.*, 2008] at the top of the Upper Red Formation in the southern Alborz, and the Red Marls in the northern Alborz. The Red Marl Formation, consists of purplish-red marine marls with intercalated limestone, sandstone, red conglomerate, basalt, and gypsum of Middle Miocene age (Langhian) [Stöcklin, 1972].

[53] Stratigraphically above Upper Red Formation, the kilometer thick sequence of coarse Hezardareh conglomerates signals intensified erosion of a steep topography in the south flank of the mountain belt, while the coarsening of deposits is even more pronounced along the northern edge of the Alborz, where conglomeratic Brown Beds (Sarmatian in age) overlie older muds. The unconformity at the base of these coarse deposits is not necessarily regionally synchronous, but it testifies to a marked increase in erosion rates over the same time interval recorded by the thermochronometry data.

[54] This most recent phase of erosional exhumation has been accompanied by an outward migration of the deformation front, manifest in the (re)activation of the Khazar Fault which served as a structural boundary and also influenced the local stratigraphy. Geological units between the current deformation front and the North Alborz Fault were a part of the South Caspian rigid block until this structural reorganization, and have not been uplifted and exhumed enough for their apatite fission tracks to be reset. Elsewhere, Morton *et al.* [2003] used provenance patterns of Pliocene sediments in the northern South Caspian Basin to argue for an increase of exhumation rates in the Greater Caucasus at roughly this time [Avdeev and Niemi, 2011]. Synchronicity of exhumation rate increases may be due to a regional reorganization of the Arabia-Eurasia collision, or to climate change, or both in combination.

5.6. Controls on the Exhumation

[55] Subdued erosion across the Alborz region during the Early Miocene, and subsidence and transgression of the Iranian interior [Şengör and Kidd, 1979] is unlikely to be attributable to an overall slow down of plate convergence, but, might be due to a change in pattern of distributed shortening across the collision zone. Distinct phases of mountain building and exhumation of the Alborz may therefore be due entirely to periodic redistribution of strain within the mountain belt rather than varying external conditions [e.g., Toussaint *et al.*, 2004]. Alternatively, active deformation may have relocated within the wider Arabia-Eurasia collision zone, which extends from the Apsheron

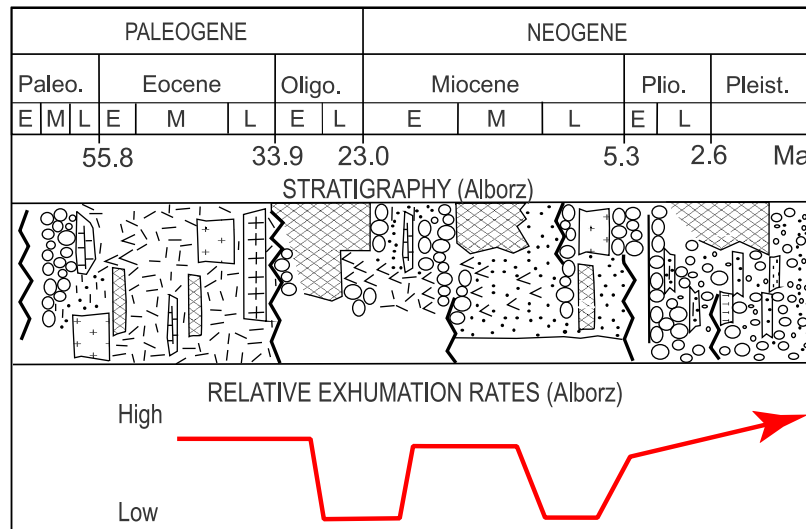


Figure 11. Summary cartoon to show relationship between Alborz stratigraphy and exhumation rates obtained by this study.

Sill in the north to the frontal structures of the Zagros in the south. It is not clear where the focus of deformation was during the Oligocene. Candidate areas include the Sanandaj-Sirjan Zone and the High Zagros, which were emergent at this time [Stöcklin, 1968]. Other possibilities include the Greater Caucasus and the Apsheron Sill, which were undergoing compressional deformation and exhumation in the Oligocene [Avdeev and Niemi, 2011; Green *et al.*, 2009; Vincent *et al.*, 2011] but this still leaves the question as to why deformation should switch away from Central Iran and the Alborz, and then switch back again.

[56] Regional re-organization of the Arabia-Eurasia collision in the last few million years has been suggested for two reasons [Allen *et al.*, 2004]. First, there are many areas within the collision zone where deformation only appears to have begun or intensified since ~ 5 Ma, including the interior of the South Caspian Basin [Devlin *et al.*, 1999] and the Greater Caucasus [Avdeev and Niemi, 2011]. At roughly the same time, compressional deformation has slowed or ceased across the interior of the Iranian plateau [Morley *et al.*, 2009]. Second, several of the major active fault systems in the collision zone need only to have been active at their present rates to achieve their total slip since the Late Miocene/early Pliocene; the North Anatolian Fault is a good example of this pattern [McClusky *et al.*, 2000]. The causes of this re-organization are not certain, given that there is no known change in overall plate convergence rate [McQuarrie *et al.*, 2003]. One possibility is that Afghan-India collision at the eastern side of the collision zone progressively prevented accommodation of Arabia-Eurasia convergence by along-strike lengthening of the collision zone [Allen *et al.*, 2011]. By contrast Avdeev and Niemi [2011] propose that final closure of the Greater Caucasus back-arc basin in late Miocene time marked the cessation of subduction of oceanic or transitional crust across much of the Arabia-Eurasia collision zone accompanied by “hard” continent-continent collision, that extended from the Arabian shield to the Scythian platform.

[57] Spatial and temporal variations of climate are unlikely to have produced all the exhumation effects referred to here and elsewhere. Notably, a strong climatic contrast between the two flanks of the mountain belt is likely to have persisted since the Miocene, with substantially wetter conditions on the northern, windward side of the range. Using oxygen isotope data from Miocene continental sedimentary deposits of the southern Alborz, Ballato *et al.* [2010] has demonstrated that the Alborz became an orographic barrier to moisture bearing northerly winds, establishing a rain shadow since ca. 17.5 Ma. Paleogeography and biostratigraphy suggest that this coincided with the final closure of the Tethyan seaway and also the beginning of isolation of the Para-Tethys from the Mediterranean Sea [Harzhauser and Piller, 2007; Harzhauser *et al.*, 2008; Reuter *et al.*, 2009]. One of the main findings in our study is less pronounced exhumation on the wet side, throughout the Neogene and earlier, which puts into question the nature and strength of a climate control on the exhumation of the mountain belt.

[58] Finally, our results show a distinct rise in exhumation rate from 6 to 4 Ma, mirrored by the stratigraphy. It has been proposed that climate may have played a role in accelerating Late Cenozoic erosion and sedimentation rates [Zhang *et al.*, 2001; Molnar, 2004] but recent work has suggested that on a global scale long-term chemical weathering fluxes, which are tied with physical erosion, have remained relatively stable since 10 Ma [Willenbring and von Blanckenburg, 2010]. For our purpose, it is the local expression of regional climate change that matters. From 5.5 Ma onward a major change in the oxygen isotope record of the Atlantic margin of Morocco indicates a dramatic change in Eurasian climate, resulting in much warmer and humid conditions. This changed the hydrological balance and resulted in a widespread transgression in the Mediterranean and the Para-Tethys but exactly how this would have impacted on the Alborz region is not yet clear. Exploration of climate change as a potential forcing mechanism affecting the exhumation and growth of the Alborz Mountains during the Neogene thus requires

more detailed constraints on the climate of the mountain belt, including contrasts between the north and south sides of bulk parameters as well as their short-term variability. Other aspects for further investigation relate to structural and lithological variations across the range, in that the southern flanks were strongly affected by Eocene extension and magmatism (Figure 4), in a way that the northern side was not. The southern regions have not been inverted to a degree that has also affected the northern side of the range.

6. Conclusions

[59] The regional thermochronometric data set produced by this study combined with outcrop geology has shown that growth of Alborz Mountains in the Cenozoic was episodic (Figure 11), with early pulses from about 60 and 35–40 Ma, followed by an interval of low level deformation between ~30–20 Ma, (Late Oligocene–Early Miocene), an acceleration in exhumation rates from ~18–20 Ma, an apparent pause from 10 to 6 Ma, and finally a major acceleration in exhumation in the Pliocene, recorded only by the AHe thermochronometer as the depth of erosion since that time has been small. Parts of these exhumation signals are in good agreement with the geological record for Central Iran, which shows a tripartite signal of terrestrial clastics (Lower Red Formation) followed by carbonates (Qom Formation) in the Late Oligocene–Early Miocene, and terrestrial clastics that continue into the Quaternary (Upper Red and Hazardareh formations) [Stöcklin, 1968; Ballato *et al.*, 2008; Morley *et al.*, 2009]. The reasons for these switches in exhumation and sedimentation are not clear. Nor is the apparent Late Miocene pause in exhumation recorded in the thermochronometry data consistent with the known stratigraphic record from Central Iran and the margins of the Alborz.

[60] There does not appear to be a single direct tectonic cause for the intensified episodic erosion, as convergence rates between Arabia and Eurasia have remained fairly constant. It may, however, relate to a change in the way convergence has been accommodated within the collision, with a shift away from the Turkish-Iranian plateau toward areas further north (Alborz, Apsheron Sill and Greater Caucasus). Climate is an alternative forcing mechanism but a paradox is that the north flank of the Alborz, which has consistently received water vapor from the adjacent Caspian Basin, since at least 17.5 Ma, would be expected to have been the focus of exhumation, and therefore be more sensitive to any changes in climate. The thermochronometric and stratigraphic data presented by this study conflict with this expectation, and indicate instead that over the long-term most erosional exhumation was located in the drier interior and south flank of the mountain belt. The explanation for this may lie with short-term observations since there is a sharp correlation between the present-day kinematic regime constrained by GPS [Djamour *et al.*, 2010] and the long-term patterns of exhumation described here. Further work on patterns and rates of short-term erosion is required to determine if present-day deformation has any bearing on the long-term records.

[61] **Acknowledgments.** The work presented in this paper has benefited from a part of PhD thesis of M. Rezaeian. She appreciates Gates foundation for funding her studies through Gates Scholarship in the University of Cambridge. We acknowledge CASP (Cambridge Arctic Shelf

Programme) has provided a few of samples. MR thanks Paolo Balloto, Ed Sobel and Saeed Madanipour for their productive and useful comments. The work would not have been possible without the assistance of Ministry of Energy of Iran (branch of TAMAB) providing unpublished data and also logistic support by the Geological Survey of Iran and National Iranian Oil Company. Nathan Niemi and two anonymous reviewers provided useful comments on the submitted version.

References

- Agard, P., J. Omrani, L. Jolivet, and F. Mouthereau (2005), Convergence history across Zagros (Iran): Constraints from collisional and earlier deformation, *Int. J. Earth Sci.*, *94*, 401–419, doi:10.1007/s00531-005-0481-4.
- Allen, M. B., and H. A. Armstrong (2008), Arabia-Eurasia collision and the forcing of mid-Cenozoic global cooling, *Paleogeogr. Paleoclim. Paleocol.*, *265*, 52–58, doi:10.1016/j.palaeo.2008.04.021.
- Allen, M. B., M. R. Ghassemi, M. Shahrabi, and M. Qorashi (2003), Accommodation of late Cenozoic oblique shortening in the Alborz range, northern Iran, *J. Struct. Geol.*, *25*, 659–672, doi:10.1016/S0191-8141(02)00064-0.
- Allen, M., J. Jackson, and R. Walker (2004), Late Cenozoic re-organization of the Arabia-Eurasia collision and the comparison of short-term and long-term deformation rates, *Tectonics*, *23*, TC2008, doi:10.1029/2003TC001530.
- Allen, M. B., M. Kheirkhah, M. H. Emami, and S. J. Jones (2011), Right-lateral shear across Iran and kinematic change in the Arabia-Eurasia collision zone, *Geophys. J. Int.*, *184*, 555–574, doi:10.1111/j.1365-246X.2010.04874.x.
- Anells, R. N., R. S. Arthurton, R. A. Bazley, and R. G. Davies (1975), Explanatory text of the Qazvin and Rasht Quadrangles map, scale 1:250000, 94 pp., Geol. Surv. of Iran, Tehran.
- Ashtari, M., D. Hatzfeld, and M. Kamalian (2005), Microseismicity in the region of Tehran, *Tectonophysics*, *395*, 193–208, doi:10.1016/j.tecto.2004.09.011.
- Avdeev, B., and N. A. Niemi (2011), Rapid Pliocene exhumation of the central Greater Caucasus constrained by low-temperature thermochronometry, *Tectonics*, *30*, TC2009, doi:10.1029/2010TC002808.
- Axen, G. J., P. J. Lam, M. Grove, D. F. Stockli, and J. Hassanzadeh (2001a), Exhumation of the west-central Alborz Mountains, Iran, Caspian subsidence, and collision-related tectonics, *Geology*, *29*, 559–562, doi:10.1130/0091-7613(2001)029<0559:EOTWCA>2.0.CO;2.
- Axen, G. J., D. F. Stockli, P. S. Lam, B. Guest, and J. Hassanzadeh (2001b), Implications of preliminary (U-Th)/He cooling ages and U/Pb crystallization ages from the Central Alborz Mountains, Iran, paper presented at Annual Meeting, Geol. Soc. of Am., Boston, Mass.
- Ballato, P., N. R. Nowaczyk, A. Landgraf, M. R. Strecker, A. Friedrich, and S. H. Tabatabaei (2008), Tectonic control on sedimentary facies pattern and sediment accumulation rates in the Miocene foreland basin of the southern Alborz mountains, northern Iran, *Tectonics*, *27*, TC6001, doi:10.1029/2008TC002278.
- Ballato, P., A. Mulch, A. Landgraf, M. R. Strecker, M. C. Dalconi, A. Friedrich, and S. H. Tabatabaei (2010), Middle to late Miocene Middle Eastern climate from stable oxygen and carbon isotope data, southern Alborz mountains, N Iran, *Earth Planet. Sci. Lett.*, *300*, 125–138, doi:10.1016/j.epsl.2010.09.043.
- Ballato, P., C. E. Uba, A. Landgraf, M. R. Strecker, M. Sudo, D. F. Stockli, A. Friedrich, and S. H. Tabatabaei (2011), Arabia-Eurasia continental collision: Insights from late Tertiary foreland-basin evolution in the Alborz mountains, northern Iran, *Geol. Soc. Am. Bull.*, *300*, 125–138, doi:10.1016/j.epsl.2010.09.043.
- Berberian, M. (1983), The southern Caspian: A compressional depression floored by a trapped, modified oceanic crust, *Can. J. Earth Sci.*, *20*, 163–183, doi:10.1139/e83-015.
- Berberian, M., and G. C. P. King (1981), Toward a paleogeography and tectonic evolution of Iran, *Can. J. Earth Sci.*, *18*, 210–265, doi:10.1139/e81-019.
- Berberian, M., and R. S. Yeats (2001), Contribution of archaeological data to studies of earthquake history in the Iranian Plateau, *J. Struct. Geol.*, *23*, 563–584, doi:10.1016/S0191-8141(00)00115-2.
- Berberian, M., M. Ghorashi, B. Arjang-Ravesh, and A. Mohajer-Ashjaei (1985), *Seismotectonic and Earthquake-Fault Hazard Investigations in the Tehran Region*, *Contrib. Seismotectonics Iran, Part V*, vol. 56, 315 pp., Geol. Surv. of Iran, Tehran.
- Berberian, M., M. Ghorashi, J. Shoja-Taheri, and M. Talebian (1996), *Seismotectonic and Earthquake-Fault Hazard Investigations in the Semnan Region*, *Contrib. Seismotectonics Iran, Part VII*, vol. 63, Geol. Surv. of Iran, Tehran.

- Bilham, R., K. Larson, and J. Freymuller (1997), GPS measurements of present-day convergence across the Nepal Himalaya, *Nature*, *386*, 61–64, doi:10.1038/386061a0.
- Brandon, M. T. (1992), Decomposition of fission-track grain-age distributions, *Am. J. Sci.*, *292*, 535–564, doi:10.2475/ajs.292.8.535.
- Brunet, M. F., and S. Cloetingh (2003), Integrated Peri-Tethyan Basins studies (Peri-Tethys Programme), *Sediment. Geol.*, *156*, 1–10, doi:10.1016/S0037-0738(02)00279-8.
- Brunet, M. F., M. V. Korotaev, A. V. Ershov, and A. M. Nikishin (2003), The South Caspian Basin: A review of its evolution from subsidence modelling, *Sediment. Geol.*, *156*, 119–148, doi:10.1016/S0037-0738(02)00285-3.
- Clark, G. C., R. G. Davies, B. Hamzpour, and C. R. Jones (1975), Explanatory text of the Bandar-e-Pahlavi quadrangle map, 1:250,000, 198 pp., Geol. Surv. of Iran, Tehran.
- Daneshian, J., and L. Ramezani Dana (2007), Early Miocene benthic foraminifera and biostratigraphy of the Qom Formation, Deh Namak, central Iran, *J. Asian Earth Sci.*, *29*, 844–858, doi:10.1016/j.jseas.2006.06.003.
- Davari, M. (1987), Geology, petrography, and petrology of Qasr-e-Firuzeh intrusive, MS thesis, Tehran Univ., Tehran.
- Davidson, J., J. Hassanzadeh, R. Berzins, D. F. Stockli, B. Bashukoo, B. Turrin, and A. Pandamouz (2004), The geology of Damavand volcano, Alborz Mountains, northern Iran, *Geol. Soc. Am. Bull.*, *116*, 16–29, doi:10.1130/B25344.1.
- Devlin, W. J., G. Cogswell, G. Gaskins, G. Isaksen, D. Pitcher, D. Puls, K. Stanley, and G. Wall (1999), South Caspian Basin: Young, cool, and full of promise, *GSA Today*, *9*, 1–9.
- Djamour, Y., et al. (2010), GPS and gravity constraints on continental deformation in the Alborz mountain range, Iran, *Geophys. J. Int.*, *183*, 1287–1301, doi:10.1111/j.1365-246X.2010.04811.x.
- Emami, M. H. (2000), Magmatism in Iran, *Tech. Rep. 71*, 608 pp., Geol. Surv. of Iran, Tehran.
- Farley, K. A. (2000), Helium diffusion from apatite: General behavior as illustrated by Durango fluoroapatite, *J. Geophys. Res.*, *105*, 2903–2914, doi:10.1029/1999JB900348.
- Farley, K. A., R. A. Wolf, and L. T. Silver (1996), The effects of long alpha-stopping distances on U-Th-He ages, *Geochim. Cosmochim. Acta*, *60*, 4223–4229, doi:10.1016/S0016-7037(96)00193-7.
- Galbraith, R. F., and P. F. Green (1990), Estimating the component ages in a finite mixture, *Nucl. Tracks Radiat. Meas.*, *17*, 197–206, doi:10.1016/1359-0189(90)90035-V.
- Galbraith, R. E., and G. M. Laslett (1993), Statistical models for mixed fission track ages, *Nucl. Tracks Radiat. Meas.*, *21*, 459–470, doi:10.1016/1359-0189(93)90185-C.
- Gautheron, C. E., L. Tassan-Got, and K. A. Farley (2006), (U–Th)/Ne chronometry, *Earth Planet. Sci. Lett.*, *243*, 520–535, doi:10.1016/j.epsl.2006.01.025.
- Geological Survey of Iran (2001), Marzan Abad sheet, in *Geological Quadrangle Map of Iran*, scale 1:100,000, edited by F. Vahdati-Daneshmand, sheet 6262, Geol. Surv. of Iran, Tehran.
- Green, T., N. Abdullayev, J. Hossack, and G. Riley, and A. M. Roberts (2009), Sedimentation and subsidence in the South Caspian Basin, Azerbaijan, *Geol. Soc. Spec. Publ.*, *312*, 241–260, doi:10.1144/SP312.12.
- Guest, B., G. J. Axen, P. S. Lam, and J. Hassanzadeh (2006a), Late Cenozoic shortening in the west-central Alborz Mountains, northern Iran, by combined conjugate strike-slip and thin-skinned deformation, *Geosphere*, *2*, 35–52, doi:10.1130/GES00019.1.
- Guest, B., D. F. Stockli, M. Grove, G. J. Axen, P. S. Lam, and J. Hassanzadeh (2006b), Thermal histories from the central Alborz Mountains, northern Iran: Implications for the spatial and temporal distribution of deformation in northern Iran, *Geol. Soc. Am. Bull.*, *118*, 1507–1521, doi:10.1130/B25819.1.
- Guest, B., B. K. Horton, G. J. Axen, J. Hassanzadeh, and W. C. McIntosh (2007), Middle to late Cenozoic basin evolution in the western Alborz Mountains: Implications for the onset of collisional deformation in northern Iran, *Tectonics*, *26*, TC6011, doi:10.1029/2006TC002091.
- Haq, B. U., and A. M. Al-Qahtani (2005), Phanerozoic cycles of sea-level change on the Arabian Platform, *GeoArabia*, *10*, 127–160.
- Harzhauser, M., and W. E. Piller (2007), Benchmark data of a changing sea—Palaeogeography, palaeobiogeography and events in the central Paratethys during the Miocene, *Palaeogeogr. Palaeoclimatol. Palaeoecol.*, *253*, 8–31, doi:10.1016/j.palaeo.2007.03.031.
- Harzhauser, M., O. Mandic, W. E. Piller, M. Reuter, and A. Kroh (2008), Tracing back the origin of the Indo-Pacific mollusc fauna: Basal Tridacninae from the Oligocene and Miocene of the sultanate of Oman, *Palaeontology*, *51*, 199–213, doi:10.1111/j.1475-4983.2007.00742.x.
- Hatzfeld, D., and P. Molnar (2010), Comparison of the kinematics and deep structures of the Zagros and Himalaya and of the Iranian and Tibetan Plateaus and geodynamic implications, *Rev. Geophys.*, *48*, RG2005, doi:10.1029/2009RG000304.
- Hessami, K., H. A. Koyi, C. J. Talbot, H. Tabasi, and E. Shabanian (2001), Progressive unconformities within an evolving foreland fold-thrust belt, Zagros Mountains, *J. Geol. Soc.*, *158*, 969–981, doi:10.1144/0016-764901-007.
- House, M. A., B. P. Wernicke, and K. A. Farley (1998), Dating topography of the Sierra Nevada, California, using apatite (U–Th)/He ages, *Nature*, *396*, 66–69, doi:10.1038/23926.
- Huber, H. (1977), Explanatory text of the Tectonic map of north-central Iran, scale 1/2,500,000, Natl. Iranian Oil Co., Tehran.
- Hurford, A. J. (1990), Standardization of fission track dating calibration: Recommendation by fission track working group of IUGS Subcommission on Geochronology, *Chem. Geol.*, *80*, 171–178.
- Hurford, A. J., and P. F. Green (1983), The zeta age calibration of fission-track dating, *Chem. Geol.*, *41*, 285–317, doi:10.1016/S0009-2541(83)80026-6.
- Jackson, J., K. Priestley, M. Allen, and M. Berberian (2002), Active tectonics of the South Caspian Basin, *Geophys. J. Int.*, *148*, 214–245.
- Ketcham, R. A. (2005), Forward and inverse modelling of low temperature thermochronometry data, in *Low-Temperature Thermochronology: Techniques, Interpretations, and Applications*, edited by P. W. Reiners and T. A. Ehlers, *Rev. Mineral. Geochem.*, vol. 58, pp. 275–314, Mineral. Soc. of Am., Chantilly, Va.
- Ketcham, R. A., A. Carter, R. A. Donelick, J. Barbarand, and A. J. Hurford (2007), Improved modelling of fission-track annealing in apatite, *Am. Mineral.*, *92*, 799–810, doi:10.2138/am.2007.2281.
- Krijgsman, W., M. Stoica, I. Vasiliev, and V. V. Popov (2010), Rise and fall of the Paratethys Sea during the Messinian salinity crisis, *Earth Planet. Sci. Lett.*, *290*(1–2), 183–191, doi:10.1016/j.epsl.2009.12.020.
- Landgraf, A., P. Ballato, M. R. Strecker, A. Friedrich, S. H. Tabatabaei, and M. Shahpasandzadeh (2009), Fault-kinematic and geomorphic observations along the North Tehran Thrust and Moshafasham Fault, Alborz mountains Iran: Implications for fault system evolution and interaction in a changing tectonic regime, *Geophys. J. Int.*, *177*, 676–690, doi:10.1111/j.1365-246X.2009.04089.x.
- Liu, M., Y. Yan, S. Stein, Y. Zhu, and J. Engeln (2000), Crustal shortening in the Andes: Why do GPS rates differ from geological rates?, *Geophys. Res. Lett.*, *27*(18), 3005–3008, doi:10.1029/2000GL008532.
- McClusky, S., et al. (2000), Global Positioning System constraints on plate kinematics and dynamics in the eastern Mediterranean and Caucasus, *J. Geophys. Res.*, *105*, 5695–5719, doi:10.1029/1996JB900351.
- McQuarrie, N., J. M. Stock, C. Verdel, and B. P. Wernicke (2003), Cenozoic evolution of Neotethys and implications for the causes of plate motions, *Geophys. Res. Lett.*, *30*(20), 2036, doi:10.1029/2003GL017992.
- Moinabadi, M. E., and A. Yassaghi (2007), Geometry and kinematics of the Moshafasham fault, south Central Alborz Range, Iran: An example of basement involved thrusting, *J. Asian Earth Sci.*, *29*, 928–938, doi:10.1016/j.jseas.2006.07.002.
- Molnar, P. (2004), Late Cenozoic increase in accumulation rates of terrestrial sediment: How might climate change have affected erosion rates?, *Annu. Rev. Earth Planet. Sci.*, *32*, 67–89, doi:10.1146/annurev.earth.32.091003.143456.
- Morley, C., B. Kongwung, A. A. Julapour, M. Abdolghafourian, M. Hajian, D. Waples, J. Warren, H. Otterdoorn, K. Srisuriyon, and H. Kazemi (2009), Structural development of the major late Cenozoic basin and transpressional belt in central Iran: The Central Basin in the Qom-Saveh area, *Geosphere*, *5*, 325–362, doi:10.1130/GES00223.1.
- Morton, A. C., M. Allen, M. D. Simmons, F. Spathopoulos, J. Still, A. Ismail-Zadeh, and S. Kroonenberg (2003), Provenance patterns in a neotectonic basin: Pliocene and Quaternary sediment supply to the South Caspian, *Basin Res.*, *15*, 321–337, doi:10.1046/j.1365-2117.2003.00208.x.
- Reiners, P. W. (2007), Thermochronologic approaches to paleotopography, in *Paleotopography: Geochemical and Thermodynamic Approaches*, *Rev. Mineral. Geochem.*, vol. 66, edited by M. J. Kohn, pp. 243–267, Mineral. Soc. of Am., Chantilly, Va.
- Reuter, M., W. E. Piller, M. Harzhauser, O. Mandic, B. Berning, F. Rögl, A. Kroh, M. P. Aubry, U. Wielandt-Schuster, and A. Hamedani (2009), The Oligo-Miocene Qom Formation (Iran): Evidence for an early Burdigalian restriction of the Tethyan seaway and closure of its Iranian gateways, *Int. J. Earth Sci.*, *98*, 627–650, doi:10.1007/s00531-007-0269-9.
- Rezaeian, M. (2008), Coupled tectonics, erosion and climate in the Alborz Mountains, PhD thesis, 237 pp., Univ. of Cambridge, Cambridge, U. K.
- Ritz, J.-F., H. Nazari, A. Ghassemi, R. Salamat, A. Shafei, S. Solaymani, and P. Vernant (2006), Active transtension inside central Alborz: A new insight into northern Iran—southern Caspian geodynamics, *Geology*, *34*, 477–480, doi:10.1130/G22319.1.
- Salehi Rad, M. R. (1979), Etud geologique de la region de Gorgan (Alborz Oriental, Iran), PhD thesis, Univ. de Paris-Sud, Paris.

- Şengör, A. M. C. (1990), A new model for the late Palaeozoic-Mesozoic tectonic evolution of Iran and implications for Oman, in *The Geology and Tectonics of the Oman Region*, edited by A. H. F. Robertson, M. P. Searle, and A. C. Ries, *Geol. Soc. Spec. Publ.*, 49, 797–831, doi:10.1144/GSL.SP.1992.049.01.49.
- Şengör, A. M. C., and W. S. F. Kidd (1979), Post-collisional tectonics of the Turkish-Iranian Plateau and a comparison with Tibet, *Tectonophysics*, 55, 361–376, doi:10.1016/0040-1951(79)90184-7.
- Stöcklin, J. (1968), Structural history and tectonics of Iran, A review, *Bull. Am. Assoc. Pet. Geol.*, 52, 1229–1258.
- Stöcklin, J. (1972), *Iran in Lexique Stratigraphique International*, vol. 3, *Asie*, 177 pp., Cent. Natl. de la Rech. Sci., Paris.
- Stöcklin, J., and J. Eftekhari-Nezhad (1969), Explanatory text of the Zanjan Quadrangle map, Rep. D4, 1:250000, 61 pp., Geol. Surv. of Iran, Tehran.
- Sussli, P. E. (1976), The geology of the lower Haraz valley area, central Alborz, Iran, technical report, 116 pp., Geol. Surv. of Iran, Tehran.
- Tatar, M., J. Jackson, D. Hatzfeld, and E. Bergman (2007), The 2004 May 28 Baladeh earthquake (Mw 6.2) in the Alborz, Iran: Overthrusting the South Caspian Basin margin, partitioning of oblique convergence and the seismic hazard of Tehran, *Geophys. J. Int.*, 170, 249–261, doi:10.1111/j.1365-246X.2007.03386.x.
- Toussaint, G., E. Burov, and P. A. Avouac (2004), Tectonic evolution of a continental collision zone: A thermomechanical numerical model, *Tectonics*, 23, TC6003, doi:10.1029/2003TC001604.
- Verdel, C. S. (2008), Cenozoic geology of Iran: An integrated study of extensional tectonics and related volcanism, PhD thesis, 182 pp., Calif. Inst. of Technol., Pasadena.
- Verdel, C. S., B. P. Wernicke, J. Hassanzadeh, and B. Guest (2011), A Paleogene extensional arc flare-up in Iran, *Tectonics*, 30, TC3008, doi:10.1029/2010TC002809.
- Vernant, P., et al. (2004), Present-day crustal deformation and plate kinematics in the Middle East constrained by GPS measurements in Iran and northern Oman, *Geophys. J. Int.*, 157, 381–398, doi:10.1111/j.1365-246X.2004.02222.x.
- Vincent, S. J., M. B. Allen, A. D. Ismail-Zadeh, R. Flecker, K. A. Foland, and M. D. Simmons (2005), Insights from the Talysh of Azerbaijan into the Paleogene evolution of the south Caspian region, *Geol. Soc. Am. Bull.*, 117, 1513–1533, doi:10.1130/B25690.1.
- Vincent, S. J., A. C. Morton, A. Carter, S. Gibbs, and T. G. Barabardze (2007), Oligocene uplift of the western Greater Caucasus: An effect of initial Arabia-Eurasia collision, *Terra Nova*, 19, 160–166, doi:10.1111/j.1365-3121.2007.00731.x.
- Vincent, S. J., A. Carter, V. Lavrishchev, T. G. Barabardze, and N. Hovius (2011), The exhumation of the western Greater Caucasus; a thermochronometric study, *Geol. Mag.*, 148, 1–21, doi:10.1017/S0016756810000257.
- Willenbring, J. K., and F. von Blanckenburg (2010), Long-term stability of global erosion rates and weathering during late-Cenozoic cooling, *Nature*, 465, 211–214, doi:10.1038/nature09044.
- Yassaghi, A., and S. Madanipour (2008), Influence of a transverse basement fault on along-strike variations in the geometry of an inverted normal fault: Case study of the Mosha Fault, *J. Struct. Geol.*, 30(12), 1507–1519, doi:10.1016/j.jsg.2008.08.006.
- Yassaghi, A., and A. Naeimi (2011), Structural analysis of the Gachsar subzone in central Alborz range; constrain for inversion tectonics followed by the range transverse faulting, *Int. J. Earth Sci.*, 100(6), 1237–1249, doi:10.1007/s00531-010-0537-y.
- Yassini, I. (1981), Paratethys Neogene deposits from the southern Caspian Sea, north Iran, *Bull. Iran. Pet. Inst.*, 83, 1–23.
- Zanchi, A., F. Berra, M. Mattei, M. Ghassemi, and J. Sabouri (2006), Inversion tectonics in central Alborz, Iran, *J. Struct. Geol.*, 28, 2023–2037, doi:10.1016/j.jsg.2006.06.020.
- Zhang, P., P. Molnar, and W. R. Downs (2001), Increased sedimentation rates and grain sizes 2–4 Myr ago due to the influence of climate change on erosion rates, *Nature*, 410, 891–897, doi:10.1038/35069099.
- Ziegler, M. A. (2001), Late Permian to Holocene paleofacies evolution of the Arabian Plate and its hydrocarbon occurrences, *GeoArabia*, 6, 445–504.

M. B. Allen, Department of Earth Sciences, Durham University, Durham DH1 3LE, UK.

A. Carter, Department of Earth and Planetary Sciences, Birbeck, University of London, Malet Street, London WC1E 7HX, UK.

N. Hovius, Department of Earth Sciences, University of Cambridge, Downing Street, Cambridge CB2 3EQ, UK.

M. Rezaeian, Department of Earth Sciences, Institute for Advanced Studies in Basic Sciences, Gava Zang, PO Box 45195-1159, Zanjan 45137-66731, Iran. (m.rezaeian@iasbs.ac.ir)